Title:

Gut microbiome-based prediction of autoimmune neuroinflammation

Authors:

Alex Steimle[1, †], Mareike Neumann[1,2 †], Erica T. Grant[1,2], Stéphanie Willieme[1], Alessandro De Sciscio[1], Amy Parrish[1,2], Markus Ollert[1,4], Eiji Miyauchi[3,5], Tomoyoshi Soga[6], Shinji Fukuda[6], Hiroshi Ohno[3] and Mahesh S. Desai[1,4]*

Affiliations:

[1] Department of Infection and Immunity, Luxembourg Institute of Health; L-4354 Esch-sur-Alzette, Luxembourg

[2] Faculty of Science, Technology and Medicine, University of Luxembourg; L-4365 Esch-sur-Alzette, Luxembourg

[3] RIKEN Center for Integrative Medical Sciences; 1-7-22 Suehiro-cho, Tsurumi-ku, Yokohama City, Kanagawa, 230-0045, Japan

[4] Department of Dermatology and Allergy Center, Odense Research Center for Anaphylaxis, University of Southern Denmark; DK-5000 Odense, Denmark

[5] Institute for Molecular and Cellular Regulation, Gunma University; 3-39-15 Showa-machi, Maebashi, Gunma, 371-8512, Japan

[6] Institute for Advanced Biosciences, Keio University, 246-2 Mizukami, Kakuganji, Tsuruoka-shi, Yamagata 997-0052, Japan

[†] These authors contributed equally

* Corresponding author. E-Mail: mahesh.desai@lih.lu

Abstract

Given the gut microbiota's contribution to pathogenesis of autoimmune diseases, microbiota characteristics could potentially be used to predict disease susceptibility or progression. Although various gut commensals have been proposed as risk factors for autoimmune disease development, predictions based on microbiota composition alone remain unreliable. Here, we evaluated a common approach to identify a potential microbial risk factor from complex communities, followed by in-depth evaluation of its risk factor properties using an autoimmune neuroinflammation disease model in mice harboring several distinct, defined microbiota compositions. We found that the relative abundances of commensal taxa across distinct communities are poorly suited to assess the disease-mediating property of a given microbiota. Instead, the presence of certain microbial risk factors allowed us to determine the probability of severe disease, but failed to predict the individual disease course. We investigated multiple other microbiota-associated characteristics by applying 16S rRNA gene sequencing, metatranscriptomic and metabolomic approaches, as well as in-depth analysis of host immune responses and intestinal barrier integrity-associated readouts. By leveraging gnotobiotic mouse models harboring six defined compositions, we identified the IgA coating index of *Bacteroides ovatus* as a reliable individual disease risk predictor before disease onset, due to its ability to reflect autoimmunity-mediating properties of a given gut microbial network within a specific host. In summary, our data suggest that common taxonomic analysis approaches should be refined by taxonomic network analyses or combined with microbiota function-related readouts to reliably assess disease predisposition of a given host−microbiota combination.

INTRODUCTION

Compared to healthy controls, autoimmune disease patients exhibit distinct microbiota compositions (*1*), especially in the context of multiple sclerosis (MS) (*2*). This observation raises the question of whether susceptibility or progression of MS can be predicted by the composition of the microbiota—which is a necessary precondition to perform patient-targeted microbiota modulations (**Fig. 1a**). A common approach to elucidate microbiota-related disease-promoting predictors uses relative abundances to identify differentially abundant bacterial taxa in MS-affected and healthy individuals, often determined by 16S rRNA gene-based sequencing (*2-9*). Although the differentially abundant taxa identified across different human cohort studies tend to be concordant, i.e. increased abundances of *Akkermansia* (*2, 4, 5, 7-9*) or decreased abundances of *Prevotella* (*3, 5-8*) in MS patients compared to healthy controls, cohort-level observations do not always explain inter-individual disease course differences. Consequently, it remains difficult to reliably link properties of the microbiota that impact MS disease course to taxonomic abundances across individuals.

Given the limitations of correlation-focused human cohort studies to uncover reliable microbial risk factors for MS susceptibility, the experimental autoimmune encephalomyelitis (EAE) mouse model (*10*) is commonly used to verify presumed causality between presence of suspected microbial risk factors and development of autoimmune neuroinflammation (*11-13*). However, by investigating properties of a singular species within only one specific background microbiota, i.e. in mice harboring a relatively consistent, specific pathogen-free (SPF) microbiota composition, conclusions from these studies are barely translateable to the plethora of individual microbiota compositions found across a given population (*1*). Although certain inter-microbial interactions promoting EAE development have previously been revealed (*11, 14*), the mutual impact between the background microbiota and potential risk commensals on disease-promoting properties of the microbiota is still poorly understood.

Considering these experimental limitations and knowledge gaps, we investigated whether the EAE disease course can be predicted before disease onset by microbiota-associated readouts. Specifically, we addressed the questions of whether taxonomic composition analyses represent appropriate tools for EAE disease prediction or whether certain microbiota-associated, functional analyses might be superior. Elaborating on these points,

67 we also examine how individual host−microbe interactions interfere with disease predictability in order to
68 guide similar attempts to predict outcomes course in other disease contexts.

RESULTS

Muc2-deficiency in mice is associated with less severe experimental autoimmune encephalomyelitis

During experimental autoimmune encephalomyelitis (EAE), the microbiota composition impacts how the host immune system is shaped (**Fig. 1a**: "Function"), resulting in variable demyelination in the central nervous system and different disease phenotypes (**Fig. 1a**). To investigate how different disease phenotypes could be predicted based on the microbiota composition (**Fig. 1a**), we first identified EAE development-associated commensal genera within a complex microbiota. To do so, we induced EAE in SPF mice of different origins, genotypes and housing conditions. Furthermore, we fed these mice diets with different fiber contents, given the impact of dietary fiber quality and quantity on relative abundances of indigenous commensals (*15, 16*). First, we addressed the question of whether changing relative abundances of taxa within a given microbiota might affect outcome of EAE. Thus, we used wildtype C57BL/6N mice purchased from Charles River (CR), which were fed either a standard laboratory chow (fiber-rich; FR) or a fiber-free diet (FF) diet for 20 days, followed by induction of EAE (**Fig. 1b**). Feeding these diets did not result in different disease outcomes (**Fig. 1c-e**), indicating that dietary fiber quantity and quality, and the associated effects on relative abundances of taxa within this particular indigenous microbiota, are not determining factors in mediating EAE (**Fig. 1f**).

Next, we wanted to elucidate whether we could observe distinct EAE outcomes between mice whose native microbiota differentiated considerably by the presence of certain taxa, rather than by relative abundances of a shared core microbiota. Thus, we induced EAE in mice deficient for the Muc2 protein ($Muc2^{-/-}$), as this genetic modification results in a significantly impaired mucus layer formation (*17*). We expected a significantly different indigenous microbiota composition due to anticipated reduction in commensals relying on an intact mucus layer as a functional or nutritional niche (*18*). As controls, we used littermate mice homozygous for *Muc2* gene presence ($Muc2^{+/+}$). While $Muc2^{+/+}$ mice were fed both FR or FF diet, $Muc2^{-/-}$ mice were only fed a FR diet (**Fig. 1g**). We observed a significant difference in disease progression between the genotypes, with $Muc2^{-/-}$ mice being significantly less susceptible to EAE induction compared to $Muc2^{+/+}$ mice, regardless of diet (**Fig. 1h-j**). As observed for CR mice (**Fig. 1f**), diet-mediated influences on disease development were negligeble (**Fig. 1k**).

Higher abundances of *Akkermansia muciniphila* are associated with less severe EAE in mice with a complex microbiota

To evaluate a potential contribution of the microbiota to the observed differences, we performed 16S rRNA gene-based sequencing analyses on DNA isolated from fecal samples taken before EAE induction (**Fig. 1l-m; Fig. S1a-f**) and during the EAE course (**Fig. S1a-e**). Since all four groups of mice expressing the Muc2 protein (CR mice and *Muc2*$^{+/+}$ mice) provided a comparable EAE disease course (**Fig. 1c, h**), which was significantly different from the one observed in *Muc2* knockout (KO) mice (**Fig. 1h)**, we compared differences between all *Muc2*-expressing mice together (WT), irrespective of origin or diet, with *Muc2*$^{-/-}$. We identified 11 differentially abundant genera that explained more than 70% of the variance detected in the Bray−Curtis distance matrix between WT and KO mice before induction of EAE (pre-EAE). Pre-EAE relative abundance of the genus *Akkermansia* alone explained 14.4% of said variance (**Fig. 1l,** right panel), correlated negatively with various EAE readouts upon induction of disease (**Fig. 1l** left panel), and were significantly higher in *Muc2*$^{-/-}$ mice compared to WT counterparts (**Fig. 1m**), suggesting disease-preventing properties of *Akkermansia* in mice.

Our observations so far are inadequate to attribute distinct EAE phenoytpes exclusively to changes in *Akkermansia* abundance, or micobiota changes in general, because potential *Muc2* knockout-associated changes in host responses were not specifically addressed. However, given that *Akkermansia* is consistently reported as a potential risk factor for MS (*2, 4, 5, 7-9*) and given its controversial role in EAE development (*2, 19*), we wondered whether these contradictory observations might be rooted in distinct background microbiota compositions.

Removal of *Akkermansia muciniphila* from a reduced microbiota results in less severe EAE

To better understand a potential causal role of *Akkermansia* in EAE development and to evaluate its potential as a disease-risk predictor, we colonized germ-free (GF) C57BL/6 mice with a 14-member human synthetic microbiota (SM14) (*15, 20*) (**Fig. 2a**). This approach allowed us to drop out specific species-of-interest from a well-characterized microbial community (SM14) to investigate the contribution of a single microbe on EAE development in a genetically homogenous host. *Akkermansia muciniphila*, the type species for the *Akkermansia* genus, is a member of this SM14 community. Thus, we colonized GF C57BL/6 mice with either

the complete SM14 community or a SM13 community, lacking *A. muciniphila*, followed by induction of EAE (**Fig. 2b**). As controls, we induced EAE in *A. muciniphila*-monoassociated (SM01) and GF mice (**Fig. S2**). While SM01-colonized and GF mice provided a low-to-intermediate EAE disease phenotype (**Fig. S2b-d**), SM13-colonized mice provided a significantly less severe EAE phenotype compared to SM14-colonized counterparts (**Fig. 2c**, left panel; **Fig. 2d-f**), highlighting the general contribution of the microbiota to EAE development and the disease-driving role of *A. muciniphila* in the SM14 microbiota-based mouse model when this species is combined with the 13 strains listed in **Fig. 2a**.

To evaluate whether changes in relative abundances of SM14-constituent strains might affect EAE disease course, we fed SM14- and SM13-colonized mice a FF diet, followed by EAE induction (**Fig. 2b**). GF mice were also fed a FF diet to exclude microbiota-independent but diet-mediated effects on EAE. Feeding SM14-colonized mice the FF diet resulted in significantly increased *A. muciniphila* relative abundances compared to equally colonized FR-fed mice (**Fig. 2g**). However, we did not detect any significant differences in any EAE-associated readout (**Fig. 2c** right panel – **Fig. 2f**) between FR- and FF-fed mice harboring the same microbiota. Removal of *A. muciniphila* from the complete SM14 community explained between 22 % and 28 % of the variance for different EAE-associated readouts (**Fig. 2e, f, Fig. S2a**). Given that SM01-colonized mice only provided an intermediate disease phenotype (**Fig. S2b-d**), we concluded that the presence of *A. muciniphila* represented a potential microbial risk factor for severe EAE when combined with other strains and that changes in its relative abundance within *A. muciniphila*-containing communities negligibly impact EAE disease course.

***Akkermansia muciniphila*-associated cecal concentrations of γ-amino butyric acid are linked to EAE severity**

To evaluate how *A. muciniphila* might alter microbiota function (**Fig. 1a**) within the SM14 reference microbiota, we performed metabolomic and metatranscriptomic analyses. EAE is associated with changes in either plasma metabolite profiles (*21, 22*) or changes in metabolic pathways of the intestinal microbiota (*23*). Furthermore, *A. muciniphila* mediates other pathologies, at least in part, via secretion of certain metabolites (*24*). Thus, we wondered whether the differences between SM14- and SM13-colonized mice could be explained by *A. muciniphila*-associated metabolite patterns in the cecum or serum. In addition to collecting cecal and serum samples from EAE- induced GF, SM01-, SM13- and SM14-colonized mice, we also collected

149 the same samples from non-EAE induced mice. Cecal metabolite profiles were similar between EAE-induced
150 and non-EAE induced groups harboring the same microbiota, as well as between EAE-induced SM13-
151 colonized and SM14-colonized mice (**Fig. 3a, b**). As these profiles were disconnected from the EAE disease
152 course (**Fig. S3a**), we hypothesized that only a few cecal metabolites, if any, might causally influence the EAE
153 disease course.

154 To identify such potential EAE-impacting metabolites, we developed a metabolite-of-interest screening
155 pipeline including 20 independent analyses (**Fig. S3b-e**). We proposed that a potential *A. muciniphila*-
156 associated and disease-mediating metabolite should fulfill five different criteria. The rationale for these criteria
157 and the analytical approach is specified in the Materials and Methods section. Among the 18 metabolites that
158 significantly correlated with at least one EAE-associated readout, only γ-amino butyric acid (GABA) emerged
159 as a metabolite-of-interest in cecal samples (**Fig. 3c**). Of note, its concentration was significantly elevated in
160 non-EAE-induced mice harboring an SM combination which resulted in severe EAE upon disease induction.
161 (**Fig. 3d**). Given that GABA concentrations were higher in disease-prone, *A. muciniphila*-harboring mice,
162 these results suggested that the cecal concentration of GABA before EAE induction already defined disease
163 development upon disease induction and that its concentration was linked to disease-influencing properties of
164 the tested microbial communities harboring *A. muciniphila*. Additionally, we did not identify any metabolite-
165 of-interest in serum samples (data not shown), indicating that potential metabolite-driven impacts on EAE
166 disease course occur locally in the intestine.

167 **Presence of *Akkermansia muciniphila* significantly alters gene expression profiles of other microbial**
168 **community members**

169 Given these community-dependent alterations in microbial metabolite profiles, we hypothesized that the
170 presence or absence of *A. muciniphila* had a significant impact on gene expression profiles of the overall
171 microbiota, possibly contributing to distinct EAE phenotypes. Thus, we performed metatranscriptomic
172 analysis of cecal contents obtained from non EAE-induced SM14- and SM13-colonized mice (**Fig. 3e-g**).
173 When comparing transcript profiles of both groups, we found 117 genes being expressed only in SM14-
174 colonized mice (**Fig. 3f**). Although we expected that these transcripts would be mostly from *A. muciniphila*,
175 in fact, most of these genes were exclusively expressed by either *Roseburia intestinalis* or *Marvinbryantia*

formatexigens (**Fig. 3g**). Of the 30 genes expressed only in SM13-colonized mice, the majority were expressed from *Eubacterium rectale* (**Fig. 3g**). These findings highlight the crucial impact of the presence of a single commensal on the gene expression pattern of other microbial community members, likely impacting their "function" (**Fig. 1a)** within a given community. These indirect influences on microbiota function might also contribute to microbiota-mediated effects on EAE development.

Mucin-degrading capacity of the microbiota is not linked to EAE severity

So far, our results suggested that predicting EAE development, based on the presence of *A. muciniphila*, was only possible in mice harboring a variation of the SM14 community (**Fig. 2, 3**) and not in mice harboring a complex community (**Fig. 1**). To further address potential reasons for these discrepancies in general, and the apparent crucial impact of *A. muciniphila* presence in SM14-colonized mice in particular, we hypothesized that changes in relative abundances of other strains, in response to *A. muciniphila* drop out from the SM14 community, might causally impact EAE development. We observed that four strains were significantly higher in abundance among SM13-colonized mice compared to SM14-colonized mice (**Fig. 4a**). To address their potential contribution to EAE development, we colonized mice with three additional SM combinations (**Fig. 4b, Fig. S4a**). In the first of these combinations, we colonized GF mice with a SM12 community (**Fig. 4b**), lacking *A. muciniphila* and *Faecalibacterium prausnitzii*. This was done to elucidate whether the > 1000-fold increase in relative abundance of *F. prausnitzii*, a species known for gut health-promoting properties (*25*) and decreased abundances in MS patients (*26*), when removing *A. muciniphila* (**Fig. 4a**) was responsible for EAE-preventing properties of the SM13 community. Intriguingly, SM12-colonized mice (**Fig. 4c-e**) provided a comparable disease course as SM13-colonized mice (**Fig. 2**), suggesting that *F. prausnitzii* expansion in SM13-colonized mice is most likely not responsible for decreased EAE in SM13-colonized mice. At the same time, these data suggest *A. muciniphila*-mediated inhibitory effects on *F. prausnitzii* expansion.

Removal of *A. muciniphila* from the SM14 community further resulted in expansion of three mucin glycan-degrading (*15*) Bacteroidetes species (**Fig. 4a**) in the SM13 community. Thus, we investigated whether colonization with the three mucin glycan-degrading strains alone (SM03) resulted in decreased EAE compared to SM14-colonized mice and whether addition of *A. muciniphila* (SM04) might counteract a potential beneficial effect. While SM03- and SM04-colonized mice showed comparable EAE disease courses (**Fig. 4c-**

e) to SM14-colonized mice (**Fig. 2**), they differed significantly from SM13-colonized mice. Additionally, the three mucin glycan-degrading Bacteroidetes strains appeared to not provide disease-reducing properties but, on the contrary, disease-promoting properties in the absence of the remaining 10 strains within the SM13 community. To evaluate whether dysregulated mucin turnover might contribute to the observed results in these mice, we assessed various indirect measures for intestinal barrier integrity. We did not detect any correlations between EAE outcome and glycan-degrading enzymatic activities (**Fig. S4b-g**), serum concentrations of LPS, occludin or ZO-1 as well as with fecal concentrations of lipocalin (**Fig. S4h,i**), or SCFA (**Fig. S4j**). Thus, we concluded that bacterially-mediated mucus glycan degradation or barrier integrity impairment was not an individual predictor for EAE disease development.

Microbiota composition can be used to estimate the probability of severe EAE incidence

Thus far, groupwise comparisons of EAE-associated readouts and microbiota compositions failed to identify reliable predictors for disease development in EAE-induced mice. Therefore, we next aimed to elucidate common denominators on a group-based and individual level to help uncover more reliable potential predictors for microbiota-mediated impacts on disease course. First, we conducted group-based comparison of EAE outcomes between all 10 tested diet−colonization combinations ("groups") (**Fig. 5a, b**). Performing hierarchical clustering (**Fig. 5c**) based on group means of key EAE-associated readouts (**Fig. 5b**) revealed three distinct group phenotypes: "moderate", "intermediate" and "severe". While diet explained less than 8 % of the variance observed for EAE-associated readouts, microbiota composition (SM) explained between 11 % and 27 % (**Fig. 5d**). Given these low η^2 values, rooted in considerable intra-group variances (**Fig. 5b**), we performed individual EAE phenotype clustering, treating all mice across all groups individually (**Fig. 5e**). T-distributed stochastic neighbor embedding (t-SNE) analysis of all EAE-induced individuals resulted in two disease clusters: "Cluster 1", comprising mice showing strong EAE symptoms, and "Cluster 2", comprising mice showing minor EAE symptoms (**Fig. 5e**). Besides SM03- and SM04-colonized mice, every group included mice of both phenotypes (**Fig. 5f**), however with varying proportions. These proportions broadly, but not completely, corresponded to the group-based phenotype classification (**Fig. 5c**). In summary, these results (**Fig. 5a-f**) indicate that knowing the composition of the microbiota, in combination with information on

dietary conditions, enables estimation of the probability for either moderate or severe disease, but is unsuitable to predict individual EAE outcomes.

Given that IL-17- and IFNγ-producing $CD4^+$ cells (*11*), $CD8^+$ cells (*27*), and IgA^+ IL-10^+ plasma cells (*28*) are reported to link the microbiota with EAE development, host-specific influences on these immune responses might contribute to individually different disease outcomes despite identical microbiome compositions. Examining such effects in more detail is critical for making disease course predictions based on microbiota composition or function. Thus, we analyzed T and B cell polarization in mice before and after EAE induction to elucidate whether potential host-specific responses occurred upstream or downstream of immune cell activation. While we detected no differences in B cell subsets among EAE-induced mice, we found 25 T cell populations in four different organs with significantly different relative abundances between groups (**Fig. 5g**, left panel; **Fig. S5a**). Among those, nine populations also correlated with individual outcome of EAE (**Fig. 5g,** left panel). Among all tested organs (colonic and ileal lamina propria, mesenteric lymph nodes and spinal cords), relative abundances of T cell populations in the spinal cords corresponded best, but not perfectly, to the respective EAE group phenotype (**Fig. 5g**, right panel**)**. While group-wise comparison of each T cell population failed to explain observed EAE phenotypes, individual cluster-based analyses (**Fig. 5e**) showed significant differences for seven populations, with IFNγ-expressing Th17 cells in the spinal cords being significantly increased in Cluster 1-mice (**Fig. 5h**). Mouse-specific T cell polarization profiles aligned better with disease outcome (**Fig. 5h**) than with SM−diet combinations (**Fig. 5h**). Thus, we concluded that host-specific differences must occur before T cell activation in EAE-induced mice, most probably due to individual microbiota-mediated signals which appeared to be distinct even in mice harboring the same set of strains.

When analyzing T cell subsets in non-EAE induced mice, we found that the microbiota composition primed $CD4^+$ T cells towards a pro-inflammatory Th17 response before EAE-induction (**Fig. S5b**). Although we found more significant correlations of these populations with EAE-associated readouts in the ileum, overall T cell population distribution in the colon aligned best with emerging EAE group phenotypes upon EAE induction (**Fig. S5c,d**), suggesting a crucial contribution of T cell priming in the colon by the microbiota to disease development upon EAE induction.

In summary, it was impossible to predict individual disease development based on microbiota−diet combinations alone despite apparent microbiota-mediated priming of the local adaptive immune system before EAE induction. This observation suggests that microbiota-mediated signals that influence the adaptive immune system to either promote or decelerate EAE development are relatively constant before disease induction, but are prone to individual changes upon disease onset.

IgA coating index of *Bacteroides ovatus* represents a surrogate measure to predict microbiota-mediated impact on individual EAE severity

Considering these individual signaling changes, we next targeted identification of microbiota-associated factors suitable to predict individual outcome of EAE. For each given strain (**Fig. 6a**), we first assessed whether its relative abundance before EAE induction (**Fig. S6a**), as determined by 16S rRNA gene sequencing in each individual mouse, allowed for prediction of individual disease course after EAE induction (**Fig. 6b, c**). To do so, we only included mice harboring at least 12 different strains, thus excluding mice with low-diversity microbiotas (SM04, SM03, SM01). Correlations for each strain were only assessed for those mice, which were gavaged with the respective strain. Although we found statistically significant correlations with EAE-associated readouts for some strains (**Fig. 6b)**, correlations were generally weak ($R<0.5$) and relative abundances of strains only explained very low proportions of the variances across all groups for several assessed EAE-associated readouts (**Fig. 6c**).

Next, we asked whether presence or absence of a given strain might be a better predictor for individual EAE development. Thus, we performed a linear mixed model regression for three EAE-associated readouts with presence of the strain as an independent variable and colonization as a random intercept effect (**Fig. 6d**, **Fig. S6b**). Given the setup of our tested SM-combination, we could only assess *A. muciniphila* and *F. prausnitzii* separately and had to analyze the remaining 12 strains in groups of two combinations. Presence or absence of a specific strain or strain combination was insufficient to predict the individual outcome of any of the tested EAE-associated readouts (**Fig. 6d, Fig. S6b**), indicating that potential disease-driving or –preventing properties of a given strain or strain combination is crucially determined by the background microbiota.

Coating of intestinal commensals by host plasma cell-derived IgA represents a crucial host response for maintaining immune homeostasis in the context of autoimmune neuroinflammation (*29-31*). Secretory IgA

(sIgA) levels in the mouse feces were disconnected from individual EAE outcomes (**Fig. S6c**), but were strongly connected to the microbiota composition (**Fig. S6d**). Interestingly, we found a significant correlation between group means of sIgA concentrations and corresponding EAE susceptibility incidence (**Fig. S6e**). Due to these observations and given that the "IgA-coating index" (ICI) was previously suggested to be a measure of autoimmunity-promoting potential of a given commensal species (*32*), we determined ICIs for each strain within each SM combination in every individual (**Fig. 6e-g, Fig. S6f**). Interestingly, the ICI of three strains, *B. caccae, B. ovatus and B. uniformis,* significantly differed between distinct SM-combinations and microbiota composition explained more than 40% of the variance between ICIs for each of these *Bacteroides* species, suggesting a crucial role of the background microbiota on strain-specific IgA coating (**Fig. S6g,h)**. Additionally, ICIs of these strains did not only vary between distinct groups, but also between individuals within groups. Thus, we hypothesized that the individual ICI of these strains might reflect individual EAE-promoting properties of the microbiota in a certain host. Correlation analysis of strain-specific ICI, as determined from fecal samples obtained before EAE induction, with EAE outcome in the same individual revealed significant correlations with some EAE-associated readouts for four strains (**Fig. 6f**). However, the only strain whose individual ICI provided significant correlations with the two most important EAE-associated readouts (AUC and maximum achieved EAE score) was *B. ovatus* (**Fig. 6f, g**), thus allowing for individual prediction of EAE disease course across all *B. ovatus*-encompassing SM combinations (**Fig. 6g**).

DISCUSSION

Given the association between the intestinal microbiota and manifestation of autoimmune neuroinflammation (*1*), microbiota manipulation might be a realistic mid-term approach to boost existing therapy options for MS patients. Potential strategies for microbiota modulation include administration of antibiotics or probiotics (*33*), dietary interventions (*34, 35*) or fecal microbiota transplantation (*36*). However, such strategies are "untargeted", leading to broad-scale changes in the microbiota with potentially unpredictable outcomes. Consequently, personalized approaches considering the unique microbiota composition in a given individual might be more promising.

A precondition for such targeted approaches is a better understanding of what exactly makes a specific microbiota composition in a given individual "disease-prone", ideally resulting in analytical procedures to evaluate the average risk of disease or even predict individual outcomes. Previously suggested measures to evaluate the MS-mediating risk of a microbial community, such as the microbiota α-diversity (*37*) or the Firmicutes-to-Bacteroidetes ratio (*38*) emerged as unsuitable tools (*26*) and more focus is now being put on individual taxa or combinations of taxa (*26*). Disease-associated bacterial taxa are often referred to as "microbial risk factors", mostly identified by differences in presence or relative abundances from cross-sectional human cohort studies.

In this study, we identified a potential autoimmune neuroinflammation-associated taxon and evaluated the quality of such a taxon-focused approach to predict disease development. One previously suggested MS-associated microbial risk factor is *Akkermansia muciniphila* (*2, 5, 7, 39*). Other studies, however, report on positive effects of *A. muciniphila* on maintaining general gut homeostasis (*40, 41*) or on progression of autoimmune neuroinflammation in mice (*19*).

At first sight, these observations might appear contradictory. They are, however, corroborated by our findings. By comparing development of experimental autoimmune encephalomyelitis (EAE) in mice of different genetic backgrounds and with distinct complex microbiotas, we found the genus *Akkermansia* to be the most negatively associated with EAE disease development, thus representing a potential hallmark genus for less severe EAE, when considering the microbiota composition as the only variable and ignoring host genetics. Next, we evaluated whether this finding could be reproduced in gnotobiotic, genetically homogenous mice

326 harboring different combinations of a reduced reference microbiota, with or without *A. muciniphila*.
327 Interestingly, we found *A. muciniphila* to be positively associated with EAE severity in certain mice harboring
328 specific reduced communities. This was associated with increased cecal levels of γ-amino butyric acid
329 (GABA). However, we cannot reliably conclude whether increased GABA concentrations are a general risk
330 factor for EAE induction or whether this only applies to a certain microbiota composition. Since elevated
331 GABA levels were previously reported to be associated with less neuroinflammation(*42, 43*), we deemed
332 assessment of intestinal GABA concentration, without corresponding information on microbiota composition,
333 unsuitable for disease course prediction. It is unclear whether this neurotransmitter directly mediates EAE-
334 influencing host responses via interaction with local host receptors (*44*) or whether it might act as a signaling
335 molecule or energy source (*45*) for other species, which finally mediate disease promotion.

336 We concluded that focusing on microbiota composition only, as we did in our experiments using mice of
337 different genotypes, can result in misleading conclusions. Co-variates, such as diet, sex, medication use,
338 geographic location, disease subtypes and genetic heterogeneity of study participants make interpretation of
339 microbiota data from human cohort studies complicated, although certain biostatistical approaches help to
340 reduce the risk of misinterpretation, as elegantly shown in a recent publication from the iMSMS Consortium
341 (*26*). In addition, we found that 16S rRNA gene sequencing-based determination of relative taxa abundances
342 is unsuitable to make meaningful assumptions on disease-mediating properties of a given microbiome.
343 Assessing the presence or absence of taxa allowed us to determine the probability of severe disease (**Fig. 6h**:
344 "Risk of disease"). However, this observation was unrelated to presence or absence of a single taxon,
345 suggesting that focusing on combinations of taxa and/or environmental factors, rather than single taxa alone,
346 may be required to form reliable conclusions.

347 Thus, we concluded that mutual influences between a suspected risk factor and the microbial environment
348 crucially shape the overall microbiota's disease-impacting potential. Results from our metatranscriptomics
349 analyses revealed that even minor changes in microbiota composition, i.e. by removing *A. muciniphila* from a
350 reduced community, resulted in profound changes in gene expression patterns of some, but not all, intestinal
351 microbes. Such influences may also affect disease-mediating properties of the microbiota, therefore we suggest
352 to put more focus on microbial network analysis to disentangle specific inter-microbial interactions. Although

353 not yet a technically and analytically refined approach (*46*), metagenomic-based microbiota network analyses
354 are currently being explored as an analysis tool (*47*) and might be superior to statistical analysis of
355 species−species co-abundances (*26*). A key study, evaluating the effects of multiple defined microbiota
356 compositions on fitness of *Drosophila melanogaster*, already pointed out that microbial network interactions
357 are more important than relative abundances of a given species alone (*48*). To the best of our knowledge, we
358 are the first to have performed a comparably complex study in a vertebrate model.

359 In addition to these microbiota-specific effects, host-specific effects also appeared to be a decisive factor for
360 individual EAE development in our experiments, further complicating the quest for reliable disease predictors.
361 Even in genetically homogenous mice of the same sex and age, harboring the exact same set of commensal
362 bacteria and living under the same standardized conditions, we found considerable individual differences in
363 EAE disease course, suggesting that the individual disease development is mediated by either
364 microbe−microbe or microbe−host interactions (*49, 50*) (**Fig. 6h**). After extensive evaluation of multiple
365 microbiota-associated readouts, we found the IgA-coating index (ICI) of *Bacteroides ovatus* to be capable of
366 "sensing" the individual EAE-influencing properties of the microbiota, irrespective of its definite composition.
367 Determining the ICI of *B. ovatus* before disease induction correctly predicted EAE outcome in every individual
368 (**Fig 6h**: "Prediction of disease"). Thus, we propose that *B. ovatus* acts as a "reporter species", reflecting the
369 individual microbiota- and host-mediated dual influences on EAE progression while taking into account
370 distinct microbiota functions across different hosts (**Fig. 6h**: "Host-mediated effects on Function"). Since this
371 property was only evaluated in reduced microbial communities, we are unable to determine whether this is a
372 SM14 community-specific observation. However, the concept of "reporter species" might also apply to other
373 strains and more complex communities, including MS patient microbiotas.

374 In summary, we demonstrate that making disease-course predictions based on microbiota characteristics is
375 generally possible, but not nearly as black-and-white as we might hope. We therefore strongly argue for a
376 reconsideration of how microbiota-related data are analyzed and interpreted. In particular, we advocate for
377 higher analytical standards, with more sophisticated data integration to better account for discrepancies in host-
378 specific microbiota function.

MATERIALS AND METHODS

Institutional Review Board Statement for conduction of mouse experiments

All mouse experiments followed a two-step animal protocol approval procedure. Protocols were first evaluated and pre-approved by either the ethical committee of the University of Luxembourg (AEEC) or the Animal Welfare System (AWS) of the Luxembourg Institute of Health, followed by final approval by the Luxembourgish Ministry of Agriculture, Viticulture, and Rural Development (Protocol numbers: LUPA2020/02, LUPA2020/27, LUPA2020/32, LUPA2019/43, LUPA2020/22, LUPA2019/51) before start of experiments. All experiments were performed according to the Federation of European Laboratory Animal Science Association (FELASA). The study was conducted according to the "Règlement grand-ducal du 11 Janvier 2013 relatif à la protection des Animaux utilisés à des fins Scientifiques" based on the "Directive 2010/63/EU" of the European Parliament and the European Council from September 2010 on the protection of animals used for scientific purposes. All animals were exposed to 12 hours of light daily.

Origin of mice and housing conditions

For gnotobiotic experiments, female germ-free (GF) C57BL/6N mice were purchased from Taconic Biosciences, Germany at the age of 4 to 8 weeks. All animals were housed and bred in the GF facility of the University of Luxembourg, supervised by the ethical committee of the University of Luxembourg (AEEC). Mice were randomly allocated to the different experimental groups and were housed in ISO-cages in groups with a maximum of five animals per cage. Water and diets were provided ad libitum. Before start of experiments, GF status of all mice was confirmed via anaerobic and aerobic microbial culturing of fecal samples in NHB and BHI liquid medium.

For experiments performed under specific pathogen-free (SPF) conditions, as shown in Fig. 1, we used female mice of different origin. C57BL/6 wildtype mice were purchased from Charles River at the age of 6 to 8 weeks. Furthermore, we used mice lacking the *Muc2* gene (strain designation: 129P2/OlaHsd×C57BL/6-Muc2<tm1Avel>), which were originally obtained from the lab of Kathy McCoy (University of Bern, Switzerland) under GF conditions. GF 129P2/OlaHsd×C57BL/6-Muc2<tm1Avel> mice were mated with SPF-housed C57BL/6 mice obtained from Charles River resulting in offspring heterozygous for presence of the *Muc2* gene ($Muc2^{+/-}$). $Muc2^{+/-}$ mice were constantly kept under the same SPF conditions as the SPF-housed

parental C57BL/6 mice. Next, male and female *Muc2*$^{+/-}$ mice were mated and offspring were genotyped for absence and presence of the *Muc2* gene. Homozygous *Muc2*$^{-/-}$ and *Muc2*$^{+/+}$ mice obtained from this breeding were then used for experiments.

Genotyping for presence or absence of the *Muc2* gene

Genotyping for presence or absence of the *Muc2* gene from mouse ear tissue was performed using the SampleIN™ Direct PCR Kit (highQu, #DPS0105) according to the manufacturer's instructions. Three different primers were used at a final concentration of 0.4 µM in the PCR reaction (Primer sequences, 5'→3'; Primer 1: TCCACATTATCACCTTGAC; Primer 2: GGATTGGGAAGACAATAG; Primer 3: AGGGAATCGGTAGACATC). The PCR was conducted with an annealing temperature of 56 °C and 37 cycles. Presence of the *Muc2* gene resulted in an amplificate of 280 bp, while absence of the *Muc2* gene resulted in an amplificate of 320 bp. Amplificates were visualized on a 1.5% agarose gel by gel electrophoresis.

Colonization of germ-free mice with a reduced human synthetic microbiota

All 14 bacterial strains of the synthetic microbiota (SM) were cultured and processed under anaerobic conditions using a Type B vinyl anaerobic chamber from LabGene, Switzerland, as published in detail previously (*20*). A total of six different SM combinations were used to colonize GF mice. Non-colonized GF mice were used as a control group. Intragastric gavage and verification of proper colonization of administered strains was performed as described in detail elsewhere (*20*). Details on the 14 different used strains are summarized in Supplementary Table 1.

Mouse diets

Mice were either maintained on a standard mouse chow (fiber-rich; "FR") or switched to a fiber-free ("FF") diet. We used two different FR diets: The FR diet used for gnotobiotic mice provided a crude fiber content of 3,9% (SAFE, Augy, France, version A04, product code U8233G10R), while the FR diet for SPF-housed mice contained a crude fiber content of 4.23% (Special Diets Service; Essex, UK; product code: 801722). The FF diet was used for both, gnotobiotic and SPF-housed mice, and was manufactured by SAFE Augy, France, based on a modified version of the Harlan TD.08810 diet as described previously (*51*). All diets were sterilized by 25 kGy gamma irradiation.

Experimental timeline of mouse experiments

Experiments performed under gnotobiotic conditions: At the age of 4 to 8 weeks, mice were colonized with various SM combination (see above), being fed a FR diet. 5 days after initial colonization, mice were either maintained on a FR diet or switched to a FF diet until the end of experiment. Mice were then either induced with experimental autoimmune encephalomyelitis (labelled as "¨+ EAE" in the manuscript) 20 days after the initial gavage or were euthanized for organ harvest 25 days after the initial gavage without induction of experimental autoimmune encephalomyelitis (labelled as "¨− EAE" in the manuscript). *Experiments performed under SPF conditions*: Mice of all genotypes were raised and maintained on a FR diet. At the age of 6 to 8 weeks, mice were either switched to a FF diet or kept on the FR diet. 20 days later, mice fed either diet were subjected to induction of experimental autoimmune encephalomyelitis (EAE). Course of EAE under both, gnotobiotic or SPF, conditions was observed for 30 days.

Experimental autoimmune encephalomyelitis (EAE)

Mice were immunized using the Hooke Kit™ MOG_{35-55}/CFA Emulsion PTX (Hooke Laboratories, Ref.: EK-2110) according to manufacturer's instructions. In brief, mice were immunized with a subcutaneous injection of a myelin oligodendrocyte glycoprotein-derived peptide (MOG_{35-55}) and complete Freund's adjuvant (CFA) delivered in pre-filled syringes. Subcutaneous injection of two times 100 µL (200 µL in total) of MOG/CFA (1 mg mL^{-1} MOG_{35-55} and 2-5 mg mL^{-1} killed mycobacterium tuberculosis H37Ra/mL (CFU)) mixture was performed on two sides bilateral in each of the mouse's flank. Additionally, Pertussis toxin (PTX) solution was injected on the day of MOG peptide immunization and 48 hours after the first injection. Glycerol-buffer stabilized PTX was diluted in sterile PBS for application of 400 ng PTX (Gnotobiotic experiments) or 150 ng (Experiments under SPF conditions) by intraperitoneal injection of 100 µL PTX solution. The EAE clinical symptom scores were assessed daily according to the scheme depicted in Extended Figure S7.

Euthanisia and organ harvest

Mice of all groups ("− EAE" and "+ EAE") were subjected to terminal anesthesia through intraperitoneal application of a combination of midazolam (5 mg kg^{-1}), ketamine (100 mg kg^{-1}), and xylazine (10 mg kg^{-1}) followed by cardiac perfusion with ice-cold PBS. Colonic content, cecal content, blood, and organs were harvested for downstream analysis. Mesenteric lymph nodes (MLN) were removed and homogenized by

mechanical passage through a 70 µm cell strainer. MLN cells were washed once in ice-cold PBS for 10 min at 800 × g, resuspended in ice-cold PBS and stored on ice until further use. Colon, ileum were removed and temporarily stored in HBSS on ice, while removed spinal cords were temporarily stored in D-PBS. All three organs were then subjected to lymphocyte extraction as decribed below.

Lymphocyte extraction from colonic lamina propria, ileal lamina propria and spinal cords

After organ removal, lymphocytes from the colonic lamina propria (CLP), ileal lamina propria (ILP) and spinal cords (SC) were extracted. While CLP and ILP lymphocytes were extracted the using the lamina propria dissociation kit (Miltenyi Biotec, Ref.: 130-097-410), SC lymphocytes were extracted using a brain dissociation kit (Miltenyi Biotec, 130-107-677) according to the manufacturer's instructions. In brief, colon and ileum were dissected and stored in modified HBSS ("HBSS (w/o)"; Hank's balanced salt solution buffered without Ca^{2+} and Mg^{2+}, buffered with 10 mM HEPES). Feces and fat tissue were removed, organs were opened longitudinally, washed in HBSS (w/o), and cut laterally into 0.5 cm long pieces. Tissue pieces were transferred into 20 mL of a predigestion solution (HBSS (w/o), 5 mM EDTA, 5% fetal bovine serum (FBS), 1 mM dithiothreitol) and kept for 20 min at 37°C under continuous rotation. Samples were then vortexed for 10 sec and applied on a 100 µm cell strainer. Last two steps were repeated once. Tissue pieces were then transferred into HBSS(w/o) and kept for 20 min at 37°C under continuous rotation. After 10 seconds of vortexing, tissue pieces were applied on a 100 µm cell strainer. Tissue pieces were then transferred to a GentleMACS C Tube (Miltenyi Biotec, Ref.: 130-093-237) containing 2.35 mL of a digestion solution and homogenized on a GentleMACS Octo Dissociator (Miltenyi Biotec, Ref. 130-096-427, program 37C_m_LPDK_1). Homogenates were resuspended in 5 mL PB Buffer (phosphate-buffered saline (PBS), pH 7.2, with 0.5 % bovine serum albumin), passed through a 70 µm cell strainer and centrifuged at 300 × g for 10 min at 4 °C. Cell pellets were resuspended in ice-cold PB buffer and stored on ice until further use. Spinal cords were stored in ice-cold D-PBS (Dulbecco's phosphate-buffered saline with calcium) until they were transferred to a GentleMACS C Tube containing a digestion solution. Samples were processed on a GentleMACS Octo Dissociator (program 37C_ABDK_01) and rinsed through a 70 µm cell strainer. The cell suspension flowthrough was then centrifuged at 300 × g for 10 min at 4 °C. Debris removal was performed by resuspending the cell pellet in 1550 µL D-PBS, adding 450 µL of Debris Removal Solution, and overlaying

with 2 mL of D-PBS. Samples were centrifuged at 4 °C at 3000 × g for 10 min. The two top phases were aspirated and the cell suspension was diluted with cold D-PBS. Samples were then inverted three times and centrifuged at 4 °C, 1000 × g for 10 min and the cell were resuspended and stored in ice-cold D-PBS until further use.

Cell stimulation and flow cytometry

10^6 cells (MLN cell suspensions as well as lymphocyte extracts from CLP, ILP and SC) were resuspended in 1 mL complete cell culture medium (RPMI containing 10% FBS, 2 mM Glutamine, 50 U mL^{-1} penicillin, 50 µg mL^{-1} streptomycin, and 0.1% mercaptoethanol) supplemented with 2 µl Cell Activation Cocktail with Brefeldin A (Biolegend Ref.: 423304) and incubated for 4 h at 37°C. Cells were centrifuged at 500 × g for 5 min and transferred into a 96-well plate. The cells were centrifuged for 5 min at 400 × g at 4°C, resuspended in 100 µL Zombie NIR (1:1000 in PBS, Zombie NIR™ Fixable Viability Kit, Biolegend, Ref: 423106) and incubated for 20 min at 4°C in the dark. Cells were washed two times with 150 µL PBS (centrifuged 5 min at 400 × g at 4°C) and resuspended in 50 µL Fc-block (1:50, Purified Rat Anti-Mouse CD16/CD32, BD, Ref.: 553142) diluted in FACS buffer (1x PBS/2% FBS/2mM, EDTA pH 8.0). Cells were incubated for 20 min at 4°C in the dark and washed two times with 150 µl PBS (centrifuged 5 min at 400 × g at 4°C). All cells were fixed for 30 min with BD Cytofix/Cytoperm solution, (BD, Ref.: 554722) and stored in PBS overnight. For the extracellular and intracellular fluorescent cell staining, cells were permeabilized with BD Perm/Wash buffer (BD, Ref.: 554723) for 15 min. T lymphocytes were evaluated using the following antibodies: rat anti-mouse IL-17A (TC11-18H10.1, 1/50; Biolegend, Ref.: 506922), rat anti-mouse RORγT (AFKJS-9, 1/44, eBiosciences, Ref.: 17-6988-82), rat anti-mouse CD3 (17A2, 1/88, Biolegend, Ref.: 100241), rat anti-mouse CD45 (30-F11, 1/88, BD, Ref.: 564225), rat anti-mouse CD4 (RM4-5, 1/700, Biolegend, Ref.: 100548), rat anti-mouse IFN-γ (XMG1.2, 1/175, eBiosciences, Ref.: 61-7311-82), rat anti-mouse Foxp3 (FJK-16s, 1/200; Thermofischer, Ref.: 48-5773-82), rat anti-mouse CD8 (53-6.7, 1/700, Biolegend, Ref.: 100710). B lymphocytes were evaluated using the following antibodies: rat anti-mouse CD19 (1D3, 1/44; eBiosciences, Ref.: 69-0193-82), rat anti-mouse CD45 (30-F11, 1/88, BD, Ref.: 564225), IgA (mA-6E1, 1/22, eBiosciences, Ref.: 11-4204-83), rat anti-mouse I-A/I-E (2G9, 1/88, BD, Ref.: 558593), rat anti-mouse CD138 (281-2, 1/22, Biolegend, Ref.: 142506), rat anti-mouse IL10 (JES5-16E3, 1/50, eBiosciences, Ref.: 45-7101-82), rat anti-

mouse CD45R/B220 (RA3-6B2, 1/88, BD, Ref.: 563893). Optimal staining concentrations of all antibodies were evaluated before staining. Cell were incubated with FACS buffer diluted antibodies for 30 min at 4°C in the dark. Samples were washed twice with 150 µl of BD Perm/Wash buffer and acquired using Quanteon NovoCyte (NovoCyte Quanteon 4025, Agilent). All acquired immunological data were analyzed using FlowJo™ Software (version 10.7.2, Becton, Dickinson, and Company; 2019). Fluorescence minus one controls (FMOs) were used for each antibody-fluorophor combination to properly evaluate signal-positive and –negative cells. Single antibody-stained UltraComp eBeads™ Compensation Beads (Fisher Scientific, Ref: 01-2222-42) were used to create the compensation matrix in FlowJo. Compensation samples were gated on the population of Compensation Beads within the FSC and SSC and the positive and negative population for the corresponding antibody were identified. After applying the compensation matrix on the samples, samples underwent the following gating strategy: (1) selecting live cells in a Zombie NIR vs. SSC plot; (2) identifying single live cells in a FSC-A vs. FSC-H plot; (3) Identifying single, live $CD45^+$ cells in a $CD45^+$ vs. FSC plot. All samples with less than 1000 events in this plot were removed from the analysis.

Illumina 16S rRNA gene sequencing and analysis

Bacterial DNA extraction from colonic and ileal content was performed as described previously (*15*). A Qubit® dsDNA HS assay kit was used to quantify sample inputs. The V4 region of the 16S rRNA gene was amplified using dual-index primers described by Kozich et al (*52*). Library preparation was performed according to manufacturer's protocol using the Quick-16S™ NGS Library Prep Kit (Zymo Research, Irvine, CA). The pooled libraries were sequenced on an Illumina MiSeq using MiSeq®Reagent Kit v2 (500-cycle) (Illumina, USA). All raw sequencing data have been uploaded to the European Nucleotide Archive (ENA) at EMBL-EBI under the study accession number PRJEB60278. The program mothur (v1.44.3) (*53*) was used to process the reads according to the MiSeq SOP (*52*). For gnotobiotic samples, taxonomy was assigned using a k-nearest neighbor consensus approach against a custom reference database corresponding to the SM14 taxa and potential contaminants (*Citrobacter rodentium*, *Lactococcus lactis* subsp. *cremoris*, *Staphylococcus aureus*, and *S. epidermis*). For SPF samples, taxonomy was assigned using the Wang approach against the SILVA v132 database. Count data was normalized by computing relative abundance.

Construction of the phylogenetic tree of SM14 constituent strains

The phylogenetic tree was constructed based on 16S rRNA gene sequences, analyzed with generous prime version 2021.2.2. Accession numbers of the used sequences were: AY271254 (*A. muciniphila*), AB510697.1 (*B. caccae*), EU136682.1 (*B. ovatus*), HQ012026.1 (*B. thetaiotaomicron*), AB050110.1 (*B. uniformis*), AB370251.1 (*B. intestinihominis*), AB626630.1 (*E. rectale*), HM245954.1 (*C. symbiosum*), AJ505973.1 (*M. formatexigens*), AF192152.1 (*D. piger*), AB011816.1 (*C. aerofaciens*), AJ413954.1 (*F. prausnitzii*), AJ312385.1 (*R. intestinalis*). Global alignment with free end and gaps, 65% similarity index cost matrix, and a Tamura-Nei genetic distance model was used to create a neighbor-joining tree build model.

Targeted metabolomics analysis of cecal contents using capillary electrophoresis-time of flight mass spectrometry (CE-TOF/MS)

Cecal metabolites were extracted from about 10 mg of a freeze-dried sample by vigorous shaking with 500 µL of 100% MeOH supplemented with 20 µM methionine sulfone as well as 20 µM D-camphor-10-sulfonic acid, as per internal standards. Four 3 mm zirconia beads (BioSpec Products, Bartlesville, OK, USA) and about 100 mg of 0.1 mm zirconia/silica beads (BioSpec Products, Bartlesville, OK, USA) were added to this mix. Afterwards, samples were shaked vigorously for 5 minutes using a Shake Master NEO (BioSpec Products, Bartlesville, Oklahoma, U.S.A.). Next, 500 µL of chloroform and 200 µL of Milli-Q water were added, and samples were shaked vigorously for 5 minutes again and followed by centrifugation (4600 × g for 30 min at 4°C). Afterwards, we transferred the obtained supernatant to a filter column with a 5 kDa cut-off (Ultrafree MC-PLHCC 250/pk) for downstream metabolite analysis (Human Metabolome Technologies, Tsuruoka, Yamagata, Japan). The resulting flow-through was vacuum dried. 50 µL of Milli-Q water containing reference compounds (200 µM 3-aminopyrrolidine and 200 µM trimesic acid) was used to dissolve the residue. The levels of extracted metabolites were measured by CE-TOF/MS in both, positive and negative modes, using an Agilent 7100 capillary electrophoresis system (Agilent Technologies, Waldbronn, Germany) equipped with an Agilent 6230 TOF LC/MS system (Agilent Technologies, Santa Clara, CA, USA).

Metabolite-of-interest screening pipeline

Given that EAE phenotypes were disconnected from the overall metabolome pattern, we looked for single metabolites which might explain observed differences in EAE disease course. Thus, we implemented a screening pipeline, comprising 20 independent analyses, to identify potential metabolites-of-interest which

might explain differences in EAE outcomes. These analyses included evaluation of the contribution of each metabolite to the variance of the PC1 and PC2 axes in a mulidimensional reduction PCA plot (**Fig. S3b**), correlation analyses (**Fig. S3c**), as well as group-wise comparisons of metabolite concentrations (**Fig. S3d**). By combining information obtained from these analyses, our goal was to shortlist microbiota-induced cecal metabolites, which enabled prediction of either the overall disease course or the relapse occurrence in EAE-induced mice. We concluded that a potential metabolite-of-interest should fulfill the following five criteria (1 − 5): (1) an overall significantly different concentration between all 7 groups (**Fig. 3c**, "SIG"; **Fig. S3e** "SIG"), as determined by one-way ANOVA tests. As we have observed differences in EAE outcome on a group-based level, this should also be reflected in different concentrations of a metabolite-of-interest between the groups. (2) a non-significant contribution to the variance of the PC2 axis (**Fig. 3c**, "PC2"; **Fig. S3b**, **Fig. S3e** "PC2_POS", "PC2_NEG"). As shown in **Fig. 3a**, different microbiota compositions were well reflected by the position of individual mice on the PC1 axis. Interestingly, differences in EAE status (EAE-induced *vs.* non-EAE-induced) were reflected by the position of individual mice on the PC2 axis. EAE-induced mice of all microbiota compositions generally provided lower values on the PC2 axis compared to their non-EAE-induced counterparts harboring the same microbiota composition. In summary, we made the following four observations (i – iv): (i) Different EAE phenotypes were a consequence of different microbiota compositions; (ii) Microbiota composition was well reflected by the position on the PC1 axis; (iii) EAE-induced mice of all microbiota compositions provided the same shift towards lower values on the PC2 axis compared to non-EAE-induced mice and (iv), as the shift towards lower values on the PC2 axis occurred in every microbiota composition, we concluded that these shifts occured independent from the EAE disease phenotype given the significant differences in EAE outcomes in mice harboring different microbiota compositions. In summary, we concluded that these shifts on the PC2 axis were either a direct result of EAE induction (independent from the disease phenotype) or a consequence of different microbiota colonization times since EAE-induced mice harbored the respective microbiota for 3 more weeks compared to non-EAE-induced mice of the same microbiota composition. Thus, we concluded that metabolites, which significantly contributed to the PC2 axis shift, were not causal to different EAE phenotypes. Instead, their concentrations in EAE-induced mice appeared to be a feedback effect from either longer colonization or EAE induction itself. In consequence, these

metabolites were removed from the list of metabolites-of-interest. (3) a significant correlation with either the overall disease course (**Fig. 3c**, "AUC"; **Fig. S3e**) or the mean score during the relapse phase (REL) in EAE-induced mice. (4) a significant correlation with the presence of *A. muciniphila* (**Fig. 3c**, "AM", **Fig. S3e**) since we observed different EAE phenotypes based on presence or absence of *A. muciniphila*. (5) a significantly different concentration when comparing non-EAE-induced mice harboring microbiota compositions leading to different EAE phenotypes upon EAE induction (**Fig 3c, Fig. S3d**). This criterion would allow for assessing the prediction aspect of cecal metabolite concentrations. As SM13-colonized and GF mice resulted in a moderate phenotype, SM01-colonized mice in an intermediate phenotype and SM14-colonized mice in a severe phenotype, we hypothesized that a potential metabolite of interest would reflect these differences by providing the following four properties (i − iv): (i) significantly different concentrations when comparing "SM13 – EAE" vs "SM14 – EAE" and "SM13 + EAE" vs "SM14 + EAE"; (ii) significantly different concentrations when comparing "SM13 – EAE" vs "SM01 – EAE" and "SM13 + EAE" vs "SM01 + EAE"; (iii) significantly different concentrations when comparing "SM01 – EAE" vs "SM14 – EAE" and "SM01 + EAE" vs "SM14 + EAE" and (iv) no significantly different concentrations when comparing "SM13 – EAE" vs "GF – EAE" and "SM13 + EAE" vs "GF + EAE".

Metatranscriptomics analysis

Flash-frozen cecal content was stored at –80°C until further processing. 1 mL RNAProtect™ (Qiagen, Ref.: 76506) was added to each sample and thawed on wet ice for 10 min. Samples were centrifuged at 10 000 × g, 4 °C for 10 min and 250 µL acid-washed glass beads (212–300 µm), 500 µL of Buffer A (0.2 M NaCl, 0.2 M Trizma base, 20 mM EDTA pH 8), 210 µL of SDS 20% and 500 µL of phenol:chloroform (125:24:1) pH 4.3 were added to the pellet. Bead‐beating on the highest frequency (30 Hz) was performed for 5 min using a mixer mill and the aqueous phase was recovered after centrifugation at 4°C for 3 min at 18 000 × g. 500 µL of phenol:chloroform (125:24:1) pH 4.3 was added to each sample and centrifuged as previously described. Again, the aqueous phase was recovered and 1/10 volume of 3M sodium acetate (pH ~ 5.5) and 1 volume of ice-cold 100% ethanol was added and gently mixed by inversion. Samples were incubated for 20 min on wet ice and then washed twice with 500 µL of ice-cold 70% ethanol and centrifuged at 4°C for 20 min at 18 000 × g. Pellets were air-dried for 10 min and resuspended in 50 µL nuclease-free water. DNase treatment was

performed by adding 10 µL 10X buffer, 40 µL nuclease-free water (to reach 100 µL final volume) and 2 µL DNase I (Thermo Scientific™ DNase I, RNase-free kit, Ref.: EN0521) followed by 30 min incubation at 37°C. 1 µL EDTA 0.5M (per sample) was added and heat-inactivated for 10 min at 65°C. RNA purification was performed with the RNeasy Mini kit (QIAGEN, Ref.: 74106) according to manufacturer instructions. RNA quantity and a quality were assessed using the RNA 6000 Nano Kit on an Agilent 2100 Bioanalyzer. Library preparation was performed using an Illumina® Stranded Total RNA Prep, Ligation with Ribo-Zero Plus kit (Illumina, Ref.: 20040529). Pooled libraries were then run on a NextSeq 550 High Output flow cell 2×75bp up to 800M reads followed by NextSeq 550 Medium Output flow cell 2x75bp up to 260M reads. RNA sequencing files were pre-processed using kneaddata (https://github.com/biobakery/kneaddata). Adapters were removed employing Trimmomatic (16). Afterwards, the fragments less than 50% of the total expected read length (75 bp) were removed. BowTie2 (17) was employed to map and filter out contaminant reads matching to either rRNA databases or the genome of *Mus musculus*. Then, clean fastq files were concatenated and passed to HUMAnN3 (18). A custom taxonomy table based on pooled 16S rRNA sequencing abundances was provided to metaPhlan for metagenome mapping. Unaligned reads were translated for protein identification using the UniRef90 database provided within HUMAnN3. Data for all samples were joined into a single table and normalized using count per million (CPM) method. Results were grouped by annotated protein product per individual. In case no annotation from UniRef90 transcript IDs was possible, distinct IDs were treated as separate gene products. Only gene products that provided >50 CPM in at least two of the eight investigated samples were included into downstream analyses. This resulted in 2213 transcripts being included into downstream analyses, representing 80 % to 85 % of the total CPM with no significant differences between the analyzed groups. CPM were recalculated to account for removed transcripts, followed by further analysis using the *edgeR* package (version 3.38.4) in R Studio (version 4.2.1). Multidimensional reduction of the transcriptome profiles was calculated using the *logFC* method within the *plotMDS.DGEList* function. Groupwise comparison of gene expression was calculated using the *exactTest()* function.

Bacterial IgA coating index

Fecal samples stored at -20 °C were resuspended in 500 µL ice-cold sterile PBS per fecal pellet and mechanically homogenized using a plastic incolulation loop. Pellets were then thoroughly shaken for 20 min

at 1100 rpm and 4 °C. After adding 2 × volume of ice-cold PBS, samples were centrifuged for 3 min at 100 × g and 4 °C to sediment undissolved debris. Clear supernatant was recovered and passed through a 70 µm sieve followed by centrifugation for 5 min at 10'000 × g and 4 °C to sediment bacteria. Supernatant was removed and pellet resuspended in 1 mL ice-cold PBS. Next, optical density of this suspension at 600 nm (OD_{600}) was detected and approximate concentration of bacteria was estimated based on the assumption that OD_{600} = 1 equals 5 × 10^8 bacteria per mL. The respective volume corresponding to 10^9 bacteria was centrifuged for 5 min at 10'000 × g and 4 °C. Pellet was then resuspended in 400 µL 5 % goat serum in PBS and incubated for 20 min on ice. After incubation, pellet was washed once in ice-cold PBS and centrifuged for 5 min at 10'000 × g and 4 °C. Pellet was then resuspended in 100 µL ice-cold PBS containing 4 µg of FITC-coupled goat anti-mouse IgA antibody (SouthernBiotech, Imtec Diagnostic, cat# 1040-02). The ratio of 4 µg of the respective antibody to stain 10^9 bacteria was previously evaluated to be the maximum amount of antibody that can be used without resulting in unspecific staining of non-IgA coated bacteria by using fecal samples from *Rag1*$^{-/-}$ mice as non IgA-coated negative controls. Samples were then incubated for 30 min at 4 °C on a shaker at 800 rpm. After incubation, 1 mL ice-cold PBS was added followed by centrifugation for 5 min at 10'000 × g and 4 °C. Samples were then washed once in ice-cold PBS, either subjected for flow-cytometry detection or for separation of IgA^+- and IgA^- bacteria. For immediate flow cytometric detection, pellets were resuspended in 200 µL DNA staining solution (0.9 % NaCl in 0.1M HEPES, pH 7.2, 1.25 µM Invitrogen SYTO™ 60 Red Fluorescent Nucleic Acid Stain) followed by incubation for 20 min on ice. After washing once with PBS, pellets were resuspended in 100 µL PBS and run immediately on a Quanteon NovoCyte (NovoCyte Quanteon 4025, Agilent). For separation of IgA^+ from IgA^- negative bacteria, we used the MACS cell separation system from Miltenyi. Pellets were resuspended in 100 µL MACS staining buffer (5 % goat serum in PBS) containing 10 µL anti-FITC microbeads (Miltenyi, #130-048-701) per 10^8 bacteria, mixed well and incubaterd for 15 min at 4 °C. After end of incubation time, 1 mL of staining buffer was added, followed by centrifugation for 5 min at 5'000 × g. Pellet was then resuspended in 5 mL staining buffer per 10^9 bacteria and loaded onto MACS LD separation columns (Miltenyi, #130-042-901) and flow-through containing the IgA^- fraction was collected. After removing columns from the magnet, the IgA^+ fraction was flushed out and collected. The IgA^+ fraction was then loaded on a MACS LS separation column (Miltenyi, #130-042-401). Flowthrough was collected and

675 combined with the previous IgA^- fraction. After removing columns from the magnet, the IgA^+ bacteria fraction
676 was flushed out, collected and combined with the previous IgA^+ fraction. Both combined fractions, IgA^+ and
677 IgA^- were then centrifuged for 10 min at 10'000 × g and 4 °C. Pellets were then resuspended in 1 mL PBS
678 and subjected to two different downstream analyses: (1) To test purity of both fractions for each sample by
679 flow cytometry, 10% of the suspension volume was used for bacterial DNA staining using SYTO™ 60 Red
680 Fluorescent Nucleic Acid Stain as described above, whereas purity was generally >90% for both fractions; (2)
681 To purify bacterial DNA for subsequent 16S rRNA gene sequencing of bacteria within the different fractions,
682 90% of the suspension volume was centrifuged for 10 min at 10'000 × g and 4 °C, supernatant was discarded
683 and the dry pellet was stored at -20 °C. DNA isolation and 16S rRNA gene sequencing was then performed as
684 described above. The IgA-coating index (*ICI*) for a given species *x* (ICI_x) was calculated by the following
685 equation, with A_x^+ representing the strain-specific relative abundance in the IgA^+ fraction and A_x^- representing
686 the strain-specific relative abundance in the IgA^- negative fraction: $ICI_x = log_{10}\left(\frac{A_x^+}{A_x^-}\right)$. Strains were classified
687 as "highly coated", when $A_x^+ > 2 \times A_x^-$ ($ICI_x > 0.301$) and as "low coated", when $ICI_x < -0.301$.

688 **Soluble IgA measurements in fecal contents**

689 We used 10 ng per well rabbit anti-mouse IgA (Novus Biologicals, # NB7506) for overnight coating of high
690 binding 384 well plates (Greiner, #781061) in 20 µl per well of carbonate-bicarbonate buffer (Sigma, #C3041).
691 Plates were then washed four times in wash buffer (10 mM Trizma Base, 154 mM NaCl, 1% (v/v) Tween-10).
692 Next, 75 µL of a blocking buffer (15 mM Trizma acetate, 136 mM NaCl, 2 mM KCl, 1% (w/v) bovine serum
693 albumin (BSA)) was added to each well and incubated for 2 h at RT. Following another washing step with was
694 buffer, samples and standards were diluted in a dilution buffer (blocking buffer + 0.1% (w/v) Tween-20). As
695 standards, we used a mouse IgA isotype control (Southern Biotech, #0106-01). 20 µL of the dilutions were
696 added to each well and incubated for 90 min at RT. Following another washing step, a secondary goat anti-
697 mouse IgA antibody, conjugated with alkaline phosphatase (Southern Biotech, # 1040-04), diluted 1:1000 in
698 dilution buffer, was added. Secondary antibody was incubated at RT for 90 min and plates were washed once.
699 As a substrate, 1 phosphate tablet (Sigma, #S0642-200 TAB) was solubilized in 1 mM 1 mM 2-Amino-2-
700 methyle-1-propanole and 0.1 mM MgCl2.6H2O. 40 µL of this substrate solution was added to each well,

701 followed by incubation at 37°C for 60 min. Final absorbance at 405 nm was detected using a SpectraMax Plus
702 384 Microplate Reader.

703 **Quantification of lipopolysaccharides levels in blood serum**

704 To quantify lipopolysaccharide levels in blood serum from mice, full blood was first incubated for 30 min at
705 37 °C, followed by centrifugation for 30 min at 3'000 × g and RT. Serum supernatant was then stored at −80
706 °C until use. Quantification was performed using the Pierce Chromogenic Endotoxin Quantification Kit
707 (ThermoScientific, #A39552) according to manufacturer's instructions. Thawed serum samples were heat-
708 shocked for 15 min at 70 °C and diluted 1:50 prior to performing the assay. After blank reduction, final
709 endotoxin levels were calculated based on detected optical densities (OD) of supplied standards and using R
710 Studio (version 4.2.1) using a 4-parameter nonlinear regression of standard ODs with the help of the *drc*
711 package (version 3.0.1) applying the function *drm(OD~concentration, fct=LL.4())*. Sample concentrations
712 were then extracted using the *ED(.., type="absolute")* function of the same package.

713 **ELISA-based quantification of zonulin and occludin concentrations in blood serum**

714 To measure concentrations of zonulin (ZO-1) and occludin (OCLN) in blood serum, we used the Mouse Tight
715 junction protein ZO-1 ELISA Kit (MyBioSource, #MBS2603798) and the Mouse Occludin (OCLN) ELISA
716 Kit (ReddotBiotech, #RD-OCLN-Mu), respectively, according to the manufacturer's instructions. After blank
717 reduction, final ZO-1 and OCLN concentrations were calculated based on detected optical densities (OD) of
718 supplied standards and using R Studio (version 4.2.1) applying a 4-parameter nonlinear regression of standard
719 ODs with the help of the *drc* package (version 3.0.1) using the function *drm(OD~concentration, fct=LL.4())*.
720 Sample concentrations were then extracted using the *ED(.., type="absolute")* function of the same package.

721 **Lipocalin-2 ELISA**

722 To measure fecal lipocalin-2 levels, the fecal pellet were homogenized in 500 µl ice-cold PBS with 1% Tween
723 20. Samples were then subjected to, agitation for 20 min at 4 °C at 2000 rpm on a thermomixer, followed by
724 centrifugation for 10 min at 21000 × g and 4°C. Pellets were discarded, supernatants were harvested and stored
725 at –20°C until further use. Final Lipocalin-2 detection was conducted using the Mouse Lipocalin-2/NGAL
726 DuoSet Elisa, R&D Systems (# DY1857) according to the manufacturer's instructions.

Detection of bacterial relative abundances using quantitative real-time PCR

To detect relative abundances of commensal bacteria from fecal samples obtained from mice harboring reduced communities (SM01 to SM14) in a gnotobiotic setting, we followed a protocol published elsewhere (*20*) without modifications. Primer sequences for strain-specific quantification are listed in Supplementary table 2.

Detection of glycan-degrading enzyme activities from mouse fecal samples

To detect activities of α-fucosidase, α-galactosidase, β-glucosidase, β-*N*-acetyl-glucosaminidase and sulfatase from fecal samples stored at −20 °C, we followed the protocol published in detail elsewhere (*54*) without modifications.

Data analysis

All figures and analyses were performed using R Studio (versions 4.1.3 and 4.2.1). For details see analysis-specific informations in this section.

Illumina 16S rRNA gene sequencing-based analysis of complex microbial communities

Groupwise analysis of taxa-annotated reads per sample was performed using R Studio (version 4.2.1). Initially, seed was set as 8765. All operational taxonomic units (OTUs) not constituting at least 0.1% of reads within at least one group (group means) were removed from the analysis. Diversity indices were determined using the *diversity()* function of the *vegan* package (version 2.6.2). Nonmetric multidimensional scaling for Bray-curtis distance matrices were calculated using the *metaMDS()* function of the *vegan* package and principal coordinate decomposition of Weighted UniFrac distance matrices were calculated the *pcoa()* function of the *ape* package (version 5.6.2). All analyses were performed on OTU level, genus level and family level. OTUs and genera contributing most to community differences between selected groups were extracted using the *simper()* function of the *vegan* package.

Acknowledgements:

We thank Kathy McCoy (University of Bern, Switzerland) for providing us with *Muc2*$^{-/-}$ mice.

Conflict of interest statement

Author M.S.D. works as a consultant and an advisory board member at Theralution GmbH, Germany.

Figure legends:

FIGURE 1:

Increased levels of *Akkermansia* are associated with lower neuroinflammation in EAE-induced mice harboring a complex native microbiota.

a) Central objective. Microbiota composition interacts with the host immune system (exhibits a specific "function"), influencing the degree of demyelination during experimental autoimmune encephalomyelitis (EAE), resulting in different disease phenotypes. Microbiota-composition based prediction of disease-mediating properties would make targeted microbiota manipulation ("Intervention") possible.

b) Experimental setting for panels c to f). C57BL/6N mice from Charles River (CR), housed under SPF conditions, were fed either a fiber-rich (FR) or fiber-free (FF) diet for 20 d, followed by induction of EAE. Mice were kept on the respective diets during EAE course. EAE disease development was observed for 30 d.

c) EAE disease scores as a function of time. All mice (FR: n=20; FF: n=19) were scored daily at the same time. Dots represent group means; shaded area and dotted lines represent SD. Statistics: daily EAE scores were compared using a Wilcoxon rank sum test. "ns": no statistical significance at any day.

d) Area-under-the-curve (AUC) analysis of the disease course depicted in c). Each mouse depicted by a separate point. Statistics: unpaired t-test after verification of normal distribution of values.

e) "Sankey" alluvial plot of key event occurrence (in % of all mice within one group) during EAE. Susceptibility: score of 2.5 for at least 1 d. Remission: decrease of EAE score by 1.5 points compared to maximum score. Relapse: Increase by 1.0 points compared to remission score.

f) Percentage of variance explained by diet when comparing AUC between FR and FF groups. Determined by eta-squared (η^2) calculation.

g) Experimental setting for panels h) to k). *Muc2*$^{+/+}$ and *Muc2*$^{-/-}$ littermate mice were fed a FR (*Muc2*$^{+/+}$ and *Muc2*$^{-/-}$) or FF (*Muc2*$^{+/+}$ only) diet for 20 d, followed by EAE induction and observation of disease course for 30 d. Mice were kept on respective diet during EAE.

h) EAE disease scores as a function of time. All mice (FR-fed *Muc2*$^{+/+}$: n=5; FF-fed *Muc2*$^{+/+}$: n=5; FR-fed *Muc2*$^{-/-}$: n=4) were scored daily at the same time. Dots represent group means; shaded area and dotted lines

represent SD. Statistics: daily EAE scores compared using a Wilcoxon rank sum test followed by "Benjamini-Hochberg" p-value correction for multiple comparisons. *:p<0.05. Grey asterics: FR-fed *Muc2*$^{-/-}$ vs FF-fed *Muc2*$^{+/+}$, Black asterics: FR-fed *Muc2*$^{-/-}$ vs FF-fed *Muc2*$^{+/+}$.

i) AUC analysis of the disease course depicted in h). Each mouse depicted by a separate point. Statistics: Tukey post-hoc test. ns: $p > 0.05$; ***: $p < 0.001$.

j) "Sankey" alluvial plot of key event occurrence (in % of all mice within one group) during EAE. Same event definition as in d).

k) Percentage of variance explained by diet and genotype when comparing AUC between the three groups depicted in h), as determined by eta-squared (η^2) calculation.

l+m) Combined analysis of microbial communities of CR mice (FF- and FR-fed), *Muc2*$^{+/+}$ mice (FF- and FR-fed) and FR-fed *Muc2*$^{-/-}$ mice as determined by Illumina-based 16S rRNA gene sequencing from fecal samples collected before EAE induction. All samples were analyzed together using the same mothur-based analysis pipeline.

l) Genera, which in summary explained more than 70% of the variance, as calculated based on Bray-Curtis dissimilarity index obtained from relative abundance data on a genus level, of fecal microbial communities between WT (CR and *Muc2*$^{+/+}$, fed both diets, combined) and KO (*Muc2*$^{-/-}$) mice before EAE induction. Squares: Spearman correlations between relative abundances of the selected genera before EAE induction with EAE-associated readouts as calculated by pairing values within each individual mouse across all five groups. Statistical significant correlations indicated by *. Bar plots depict cumulative explained variance for combinations of genera, ordered from bottom (highest single contribution) to top (lowest single contribution).

m) Relative abundances of the genus *Akkermansia* in fecal microbial communities before EAE induction. Statistics: Tukey post-hoc test. Non-significant comparisons not shown. *: $p < 0.05$; **: $p < 0.01$; ****: $p < 0.0001$.

FIGURE 2:

Removing *Akkermansia muciniphila* from a standardized reduced microbiota results in reduced neuroinflammation in EAE-induced mice.

a) Phylogenetic relation between strains comprising the SM14 community (see Materials and Methods for strain designations and construction of the phylogenetic tree).

b) Experimental setup. GF C57BL/6 mice were colonized with either SM14 or SM13 (SM14 w/o *A. muciniphila*) communities. 5 d after initial colonization, mice harboring both SM combinations were either switched to a fiber-free (FF) diet or were maintained on a standard chow (FR). 20 d after diet switch, EAE was induced in all mice and disease course was observed for 30 d.

c) EAE disease scores as a function of time. All mice (FR-fed SM14: n=13; FR-fed SM13: n=11, FF-fed SM14: n=10, FF-fed SM13: n=4) were scored daily at the same time. Left panel: FR-fed mice. Right panel: FF-fed mice. Dotted lines represent SD. Statistics: daily EAE scores were compared using a Wilcoxon rank sum test. Left panel: * indicates $p < 0.05$ when comparing SM14- with SM13-colonized mice (FR-fed only). Right panel: "ns" indicates $p>0.05$ on any given day when comparing FR- with FF-fed mice harboring the same SM combinations.

d) "Sankey" alluvial plot of key event occurrence (in % of all mice within one group) during EAE. Same event definition as in Fig. 1e.

e) Left panel: Area-under-the-curve (AUC) analysis of the disease course depicted in c). Each mouse depicted by a separate point. Statistics: One-Way ANOVA followed by Tukey's post-hoc test. ns: $p > 0.05$; * < 0.05. Right panel: Percentage of variance explained (eta-squared (η^2)) by diet or colonization (SM combinations; "SM") when comparing AUC between all 4 groups depicted in the left panel.

f) Left panel: Mean EAE score during relapse phase (day 26 to day 30). Each mouse depicted by a separate point. Statistics: One-Way ANOVA followed by Tukey's post-hoc test. ns: $p > 0.05$; * < 0.05. Right panel: eta-squared analysis as decribed in e).

g) Streamcharts of relative bacterial abundances as a function of time (days after EAE induction). Mean relative abundances per strain, group and timepoint are shown. 2-letter abbreviations of SM14- and SM13-

828 constituent strains are explained in panel a). Bacterial relative abundances were determined by 16S rRNA gene

829 based sequencing.

FIGURE 3:

***Akkermansia muciniphila*-mediated autoimmune neuroinflammation is associated with increased cecal concentrations of γ-amino butyric acid**

a-d): Identification of microbiota-induced and EAE disease course-influencing metabolites using a metabolite screening pipeline. Germ-free (GF) C57BL/6 mice were either colonized with *Akkermansia muciniphila* only (SM01), the 13SM community (SM13), the 14SM community (SM14) or remained GF. 25d after initial colonization, mice were either subjected to harvesting cecal contents ("− EAE", n = 4 per group) or were EAE-induced followed by cecal content harvest 30d after EAE induction ("+ EAE", n = 4 per group). Cecal contents were subjected to targeted GC/MS-TOF-based metabolomics analysis. A total of 175 metabolites were identified in at least 50% of the samples in at least one group and were thus included in the overall analysis pipeline.

a): Principal component analysis (PCA) of log-normalized metabolite concentrations using a Euclidian distance matrix. Panels separated by microbiota compositions.

b) Hierachical clustering of the 7 groups based on scaled group means of log-normalized concentrations of each detected metabolite.

c) "Criteria intersection analysis" of the 175 detected metabolites. Criteria were categorized into "correlation criteria", summarizing the results of either statistically significant positive ("PCor") or statistically significant negative Spearman correlation ("NCor") across all samples of all groups (both, EAE-induced and non-induced mice) and "groupwise comparison criteria". Correlations referring to EAE-associated criteria ("AUC": Area under the curve of the disease course, "MAX": maximum EAE score, "SUS": susceptibility to EAE induction as defined in Fig 1c, "REL": occurrence of relapse during the last 5 days of EAE course as defined in Fig 1c) were calculated using samples of EAE-induced mice only. Groupwise comparisons include metabolites found to be significantly different between two given groups based on an unpaired t-tests of log-normalized concentrations, using a "Benjamini-Hochberg" ("BH")-corrected adjusted p-value (p.adjust) as significance criterion. Bar plots indicate the total number of metabolites which fulfill each listed criterion. Of the total 175 metabolites, only the criteria intersections of the 18 metabolites, which provide a significant correlation with either AUC or REL (or both), are displayed in detail. Grey squares indicate that a given metabolite (on the y-

857 axis) fulfilled a specific criterion (on the x-axis) while a white square indicate a failure to fulfill a given
858 criterion.

859 **d)** Boxplots of log-normalized concentrations of γ-amino butyric acid (GABA) under EAE or non-EAE
860 induced conditions. Statistics were calculated using am unpaired t-test with a "BH" correction for multiple
861 comparisons.

862 **e-g):** Metatranscriptomic analysis of cecal contents of non-EAE-induced SM14-colonized (n=4) and SM13-
863 colonized (n=4) mice. Analysis includes 2213 product-annotated transcripts, surpassing a threshold of 50 CPM
864 in at least 2 samples, accounting for 80 % to 85% of the total CPM.

865 **e):** Multidimensional reduction of transcriptome profiles. In case of SM14-colonized mice, all product-
866 annotated transcripts predicted to be derived from *A. muciniphila* were removed and CPM in these samples
867 were recalculated. This allowed to compare transcriptome profiles of SM13-constituent strains in absence and
868 presence of *A. muciniphila*.

869 **f**): Volcano plot with each dot representing one transcript. Log_2-transformed ratio of fold-change (FC) relative
870 transcript abundance (Log_2FC) in SM14-colonized mice compared to SM13-colonized mice shown on the x-
871 axis. P value of the respective log-transformed FC shown on the y-axis. Dotted line represents significance
872 threshold ($p > 0.05$). Yellow dots represent product-annotated transcripts only found in SM14-colonized mice
873 (Group CPM mean > 10). Blue dots represent product-annotated transcripts only found in SM13-colonized
874 mice. Grey dots represent product-annotated transcripts found in both groups. n represents number of product-
875 annotated transcripts.

876 **g**): Left 2 panels: Number (n) of genes and cumulative CPM (× 1000) of transcripts being expressed only in
877 either SM13-colonized or SM14-colonized mice. Right 2 panels: Number (n) of genes and cumulative CPM (
878 × 1000) of transcripts being either upregulated or downregulated in SM14-colonized mice, but present in both,
879 SM14- and SM13-colonized mice.

FIGURE 4:

Mucin-degrading capacity of the microbiota is disconnected from EAE disease course

a) 16S rRNA gene based sequencing. Relative abundances of strains, which provided statistically significant differences between FR-fed SM14-colonized mice and FR-fed SM13-colonized mice, as determined by one-way ANOVA followed by Tukey's post-hoc test, on the day of EAE induction ("before EAE"). *: $0.01 < p < 0.05$; **: $0.001 < p < 0.01$; ***: $p < 0.001$.

b) Summary of constituent strains of all used SM communities. Two-letter abbreviations explained in Fig. 2a.

c) EAE disease scores as a function of time. All mice (FR-fed SM03: n=5; FR-fed SM04: n=5, FR-fed SM12: n=4) were scored daily at the same time. Statistics: daily EAE scores were compared using a Wilcoxon rank sum test with a "BH" correction for multiple comparisons. Blue asterisks represent comparison with FR-fed SM13-colonized mice, yellow asterisks with FR-fed SM14-colonized mice. * indicates $p < 0.05$.

d) "Sankey" alluvial plot of key event occurrence (in % of all mice within one group) during EAE. Same event definition as in Fig. 1e.

e) Left panel: Area-under-the-curve (AUC) analysis of the disease course depicted in c). Each mouse depicted by a separate point. Middle panel: Maximum EAE score per mouse. Right panel: Mean EAE score during relapse phase (d 26 to d 30). Statistics: One-Way ANOVA followed by Tukey's post-hoc test. Blue font indicates comparison with FR-fed SM13-colonized mice, yellow font with FR-fed SM14-colonized mice. *: $0.01 < p < 0.05$, **: $p < 0.01$.

FIGURE 5:

Microbiota alterations result in three different EAE group phenotypes and two different individual phenotypes

a) Summary of EAE disease course of all tested colonization/diet-combinations. Heatmap summarizes data from Fig. 2c, S2 and 4c. Daily mean EAE score per colonization/diet-combination visualized by color scale.

b) Summary of key EAE-associated readouts of all tested colonization/diet-combinations. Squares indicate group mean. Dark grey bar indicates standard deviation (SD). For definition of "Susceptibility", "Relapse Incidence" and "Remission Incidence" see Fig. 1d.

c) Groupwise EAE phenotype classification. Cluster dendrogram of scaled group means of EAE-associated readouts (panel b), based on a Euclidian distance matrix. Group phenotypes were classified according to the three obtained main clusters.

d) Percentage of variance explained (eta-squared (η^2)) by diet or SM-combinations (SM) when comparing EAE-associated readouts among all colonization/diet-combinations.

e) EAE phenotype classification by mouse ("Individual") by applying t-stochastic neighbor embedding (t-SNE) analysis to EAE-associated readouts data sets of each individual mouse across all tested colonization/diet-combinations. Cluster 1 (strong EAE symptoms) and Cluster 2 (minor EAE symptoms) phenotype) resulted from applying a perplexity of 20 to t-SNE analysis, using 6 initial dimensions.

f) Proportion of mice in Cluster 1 per colonization/diet-combination.

g) Upper panel: Relative abundances of T cell subsets [%CD45], scaled by subset and organ, of those subsets which provided significant differences as determined by one-way Anova. Lower panel: Correlations between relative abundances of those subsets with key EAE-associated readouts in the same individuals. All mice of all groups included irrespective of microbiota composition. Right: Hierarchical group clustering of all 10 tested colonization-diet combinations based on subset means of significantly different T cell subsets in the spinal cords.

h) Relative abundances of T cell subsets which were found to be statistically significant by EAE phenotype cluster affiliation, as determined by unpaired t-tests. *: $0.01 < p < 0.05$; **: $p < 0.01$.

924 **FIGURE 6:**

925 **Using IgA coating index of an inert reporter species as surrogate measure to assess EAE-mediating**
926 **properties of a given microbial community**

927 **a)**: Color codes and 2-letter abbreviations of all SM14-constituent strains

928 **b)**: Pearson correlation matrix between bacterial relative abundance of each strain before EAE induction
929 (horizontal), as detected by 16S rRNA gene sequencing, with several EAE-associated readouts (vertical) for
930 individual mice: AUC = area under the curve (panel e). Max = maximum EAE score. RelM = Mean EAE score
931 during relapse phase, RemO = Occurrence of remssion, SusO = Susceptibility. For AM, only SM14-colonized
932 mice were included in the calculation. For FP, only SM13- and SM14-colonized mice were included, for all
933 other strains SM14-, SM13-, and SM12-colonized mice were included. Mice of both dietary groups were
934 included in this analysis. *: $p < 0.05$ (without further distinction).

935 **c)**: Variance of three key EAE-associated readouts explained by relative abundance of a given strain before
936 EAE induction.

937 **d)**: Linear mixed model regression for predicted AUC with presence of the strain as an independent variable
938 and colonization as a random intercept effect.

939 **e):** Variance in IgA-coating index (ICI) explained by background microbiota compositions in three strains
940 providing highest microbiota-dependencies on ICI.

941 **f):** Individual-based paired Pearson correlation of key EAE associated readouts with ICIs of SM14-constituent
942 strains before EAE induction. Mice of all colonization-diet combinations were included into this analysis. *:
943 $p < 0.05$ (without further distinction).

944 **g):** Correlation of *B. ovatus* ICI with AUC (left) and maximum EAE score (right) in all mice harboring *B.*
945 *ovatus*, irrespective of background microbiota.

946 **h)**: Final conclusion. Taxonomic microbiota information can be used to assess the "Risk" of a given individual
947 to develop disease (as defined by a chance < 100 %). For "Predictions", as defined by a 100 % chance to
948 develop disease, host-mediated influences on the microbiota function within a given individual must have to
949 be taken into account.

EXTENDED FIGURE S1

OTU level-based microbiota analysis of SPF-housed mice

16S rRNA gene-based sequencing analyses of DNA isolated from fecal samples. All samples were analyzed together using the same mothur-based analysis pipeline. Only those OTUs that provided a mean relative abundance of at least 0.01% in at least one group were included.

a-b): Multidimensional reduction (**a:** NMDS plot based on a Bray-Curtis distance matrix; **b:** Principal coordinate analysis (PCoA) using a weighted UniFrac distance matrix) of microbiota composition based on OTUs. Fecal samples collected the day before EAE induction. Left panels show clustering of samples by group, middle and right panel depict the same samples on the same two-dimensional scale as the left panel, colored by susceptibility to EAE or occurrence of relapse in the mouse the respective sample was obtained from. Ellipses represent 95% confidence interval for each group. The minor differences between groups in **b**), compared to more prominent differences between groups in **a**) indicate that the detected differences in the NMDS plot (**a**) are mostly based on phylogenetically related OTUs.

c-d): Multidimensional reduction (**c:** NMDS plot based on a Bray-Curtis distance matrix; **d:** Principal coordinate analysis (PCoA) using a weighted UniFrac distance matrix) of microbiota composition based on OTUs. Fecal samples collected at day 10 to 18 ("MID") or at day 30 ("END") after EAE induction. Ellipses represent 95% confidence interval for each group. Detected shifts during EAE disease course using both methods of multivariate reductions were disconnected from group EAE phenotype (**Fig. 1**).

e): Alpha-diversity analysis of microbiota composition before and during EAE, separated by groups and diversity indices. Fecal samples collected the day before EAE induction ("START"), at day 10 to 18 ("MID") or at day 30 ("END") after EAE induction. InvSimpson = inverse Simpson index; Observations = number of detected taxa (OTUs); Shannon = Shannon diversity index.

f) Intersection analysis to identify taxa, which are either present or absent only in *Muc2*$^{-/-}$ mice. Taxa were considered "present" within a certain group, when group mean relative abundance of a given taxon was > 0.01%. Otherwise, taxa were considered "absent" in the respective group. Red: taxa only present in *Muc2*$^{-/-}$ mice; teal: taxa not present in *Muc2*$^{-/-}$ mice, but in all other mice; orange: core microbiome shared by mice of all five groups.

977 **EXTENDED FIGURE S2**

978 **EAE disease course in GF as well as SM01-, SM13- and SM14-colonized mice**

979 **a):** Left panel: Percentage of variance explained by diet and SM combination (SM) as determined by eta-
980 squared (η^2) calculation when comparing the maximum achieved EAE score during the 30 d disease
981 observation period between FR- and FF-fed SM14- and SM13-colonized mice. Right panel: Maximum
982 achieved EAE score per group. Each mouse depicted by a separate point in the boxplot. Statistics: One-Way
983 ANOVA followed by Tukey's post-hoc test. No statistically different group differences observed.

984 **b-d):** GF C57BL/6 mice were either monocolonized with *A. muciniphila* (SM01) or remained GF. GF mice
985 were fed either a FF or a FR diet. SM01 mice were only fed a FR diet. EAE was induced in GF mice 20 d after
986 diet switch. EAE was induced in SM01-colonized mice 25 d after initial colonization. Disease course in all
987 groups was observed for 30 days.

988 **b):** EAE disease scores as a function of time. All mice (FR-fed GF: n=4; FR-fed GF: n=4, FR-fed SM01: n=5).
989 Dots represent daily group means. Dotted lines represent SD.

990 **c):** Sankey" alluvial plot of key event occurrence (in % of all mice within one group) during EAE. Same event
991 definition as in Fig. 1e.

992 **d):** Area-under-the-curve (AUC) analysis of the disease course depicted in b). Each mouse depicted by a
993 separate point.

EXTENDED FIGURE S3

Metabolite-of-interest analysis pipeline

a): Principal component analysis (PCA) of log-normalized metabolite concentrations using a Euclidian distance matrix. Each dot represents an EAE-induced individual mouse, independent of microbiota composition. Dot colors represent EAE severity in each individual mouse, with strong EAE phenotypes colored in red. Severity represented by either AUC values of the individual EAE disease course as a function of time (left panel) or the mean score during the relapse phase (REL; right panel). EAE phenotypes, as indicated by the area-under-the curve of EAE disease courses (AUC) and mean scores during relapse phase (REL), were disconnected from the overall metabolome pattern.

b): Biplot showing the loadings of each metabolite, indicating positive or negative contribution to PC1 and PC2 axes. Each metabolite represented by one dot. Metabolites were classified as having a significant contribution (colored with red circles or white circles with red outline) when their loadings were either smaller than −0.09 or higher than +0.09 for both, PC1 and PC2. Metabolites are listed under their KEGG-ID. A list of metabolite names with corresponding KEGG-IDs is provided in **Supplementary table 3**.

c): Pearson correlation of metabolite concentrations with key EAE-associated readouts. Only samples from EAE-induced mice were used for analysis. Significant correlations are shown in either blue (positive) or red (negative). Non-significant correlations were removed from the figure.

d): Volcano plot of groupwise comparison between the groups as indicated by the color-coded legend. Significantly different expressed metabolites are shown in red. Benjamini-Hochberg correction was used to adjust p-values.

e): Criteria intersection analysis" of all 175 detected metabolites. Metabolites are listed under their KEGG-ID. A list of metabolite names with corresponding KEGG-IDs is provided in **Supplementary table 3.** Fulfilled criteria indicated by a grey square; not fulfilled criteria by a white square. Criteria were categorized into "correlation criteria", summarizing the results of either statistically significant positive ("PCor") or statistically significant negative Spearman correlation ("NCor") across all samples of all groups (both, EAE-induced and non-induced mice) and "groupwise comparison criteria". Correlations referring to EAE-associated criteria ("AUC": Area under the curve of the disease course, "MAX": maximum EAE score, "SUS": susceptibility to

EAE induction as defined in Fig 1c, "REL": occurrence of relapse during the last 5 days of EAE course as defined in Fig 1e) were calculated using samples of EAE-induced mice only. Groupwise comparisons include metabolites found to be significantly different between two given groups based on an unpaired t-tests of log-normalized concentrations, using a "Benjamini-Hochberg" ("BH")-corrected adjusted p-value (p.adjust) as significance criterion.

EXTENDED FIGURE S4

Analysis of barrier integrity and mucin-associated glycan degrading capacities of reduced microbiota compositions

a): Colonization verification. Relative abundance of bacterial strains in SM03-, SM04- and SM12-colonized mice after initial colonization as detected by qPCR using strain-specific primers.

b – g): Given that two of the three SM combinations which resulted in a "severe" phenotype (**Fig. 4c, Fig. 5c**) comprised the full set of mucin glycan-degrading strains (*A. muciniphila, B. caccae, B. instinihominis, B. thetaiotaomicron*) within the SM14 community and given that increased activities of microbial mucin-glycan degrading enzymes, as detected from fecal samples, were previously reported to be associated with increased susceptiblity towards enteropathogenic infections (*15*), we wondered whether altered activities of these enzymes might also contribute to different EAE disease outcomes. Thus, we detected activities of *N*-acetylglucosaminidase (Nag), α-fucosidase (Fuc) and sulfatase (Sulf) (*54*), which are involved in degradation of mucin-associated glycan structures (*15*). As controls, we also detected activities of enzymes involved in fermentation of mostly plant-derived fiber structures: α-glucosidase (Gluc) and β-galactosidase (Gal). Enzyme activities were measured at three different timepoints during the 30 d of EAE disease course, which we called "periods": Before EAE induction ("Start"), during the phase with the maximum EAE score ("Peak") which corresponded to day 14 to day 20, dependent on the individual, as well as during the remission phase ("Rem") which corresponded to day 21 to day 25 after EAE induction.

b): Enzyme activities of of *N*-acetylglucosaminidase (Nag), α-fucosidase (Fuc) and sulfatase (Sulf), α-glucosidase (Gluc) and β-galactosidase (Gal) as determined from fecal samples collected either before EAE induction (Start), during peak (Peak) or remission phase (Rem). Peak = day 14 to day 20 after EAE induction. Rem = day 20 to day 25 after EAE induction.

c): Enzyme activities of of *N*-acetylglucosaminidase (Nag), α-fucosidase (Fuc) and sulfatase (Sulf), α-glucosidase (Gluc) and β-galactosidase (Gal) as determined from fecal samples in EAE-induced mice, based on cluster affiliation and period after EAE induction. Same period definition as in **Fig. S4a**. Same cluster definition as in **Fig. 5e**.

d): Variance in enzymatic activities Fuc, Nag, Sulf, Gluc and Gal, as determined from fecal samples of EAE-induced mice, explained by microbiota composition (Col), diet or period after EAE induction (Start; Peak; Remission; Relapse = day 26 to day 30 after EAE induction). While the microbiota composition turned out to be most determining factor for the different enzyme activities, diet only explained a considerable proportion of the variance for the two plant glycan-derived fiber degrading enzymes Gluc and Gal. The timepoint of sampling EAE course explained between 9 % and 16 % of the variances, suggesting that enzyme activities are, at least in part, either impacted by the current state of neuroinflammation or involved in mediating the current state of neuroinflammation

e): Pearson correlation coefficients of enzymatic activities Fuc, Nag, Sulf, Gluc and Gal, as determined from fecal samples of EAE-induced mice with EAE score at the same day of fecal sampling. Separated by microbiota composition. Upper panel: all mice of all microbiota-diet combinations combined ("All groups"). Lower panel: those mice included into correlation analyses which belong to the indicated diet-colonization combinations. Statistically significant correlations ($p < 0.05$) are marked with *. Only Nag activities correlated significantly with EAE scores at the same day when considering all mice independent from the microbiota composition. We observed considerable differences when including only mice harboring the same microbiota composition, or the same diet or both, into such analyses (lower panel), highlighting that enzyme activity-EAE readout correlations strongly depended on the microbiota composition.

f): Pearson's coefficients of correlations of enzymatic activities Fuc, Nag, Sulf, Gluc and Gal in fecal samples of EAE-induced mice before EAE induction with key EAE-associated readouts after EAE-induction in the same individuals. No statistically significant correlations were determined. No enzyme could predict any of the six key EAE-associated readouts when considering all mice of all colonization-diet combinations

g): Pearson's coefficients of correlations of enzyme activities during Peak phase with EAE scores during remission phase of the same indiviuals. Mice from all microbiota-diet combinations combined. Only Nag activites during the Peak phase could be used to predict EAE scores during the remission phase. Nag activities correlated positively with higher EAE scores, or in other words, less remission. This correlation was significant, but relatively weak.

h – j): Given the significant correlation of Nag activities with certain EAE-associated readouts, we next addressed whether increased Nag activities might contribute to decreased mucosal barrier integrity and whether this might impact EAE development. It has previously been shown that increased Nag activities were associated with impairment of the intestinal mucus layer and increased lipocalin secretion into the intestinal lumen (*15*). Furthermore, reduced mucosal barrier integrity is discussed as a contributing factor to MS pathology (*55, 56*). Since we did not assess mucus layer thickness directly, we detected indirect measures of mucosal barrier integrity, such as serum levels of lipopolysaccharides (LPS), occludin and zonulin, as well as lipocalin concentrations from fecal samples. Additionally, we assessed short-chain fatty acid (SCFAs) concentrations given their contribution to maintenance of mucosal barrier integrity (*57, 58*) and the disease-alleviating properties of propionate in patients (*4*) and mice (*59*).

h): Fecal concentrations of lipocalin (LCN) and serum concentrations of lipopolysaccharide (LPS), occludin (OCCL) and zonulin (ZO-1) as determined from before EAE induction (−EAE) or 30 d after EAE-induction (+EAE) in EAE-induced mice. Some group/readout/timepoint combinations were not determined.

i): Pearson's coefficients of correlations between fecal LCN concentrations, serum OCCL concentrations, serum LPS concentrations and serum LCN concentrations before induction of EAE with key EAE-associated readouts in the same individual across all tested microbiota-diet combinations. No statistically significant correlations could be determined.

j): Fecal concentrations of short-chain fatty acids in non-EAE induced mice of certain microbiota-diet combinations. SCFA concentrations were completely unrelated to EAE disease phenotypes upon EAE induction.

EXTENDED FIGURE S5

T cell polarisation in EAE-induced and non-EAE-induced mice

a): Boxplots of relative abundances of certain T cell populations in various organs. Group means of these populations are summarized in the heatmap shown in **Fig. 5g**. Colon, ileum, mesenteric lymphnodes and spinal cords were harvested followed by isolation of lymphocytes. Isolated lymphocates were subjected to flow cytometry-based analyses and relative abundances of subpopulations were calculated as percentage of CD45-expressing cells. LP = lamina propria. Each dot represents one invidual. Groups are arranged based on their EAE group phenotype classification (**Fig. 5c**). Severe phenotype on the left: FR-fed SM04 ("SM04 FR"), FR-fed SM03 ("SM03 FR"), FR-fed SM14 ("SM14 FR"). Intermediate phenotype in the middle: FR-fed SM01 ("SM01 FR"), FF-fed SM14 ("SM14 FF"). Moderate phenotype on the right: FF-fed germ-free mice ("GF FF"), FF-fed SM13 ("SM13 FF"), FR-fed SM13 ("SM13 FR"), FR-fed germ-free ("GF FR"), FR-fed SM12 ("SM12 FRF"). Statistics: only population-organ combinations with statistically significant differences, as calculated by ANOVA, are shown. Tukey's honestly significant difference tests (Tukey HSD) were applied to subsequently determine statistical different value distribution between all groups within each population-organ combination. Statistical differences are indicated by group-assigned letters (a – d). Two groups sharing an assigned letter: $p > 0.05$. Two groups not sharing an assigned letter: $p < 0.05$ (without further distinction).

b – d): Analysis of T cell populations in non EAE-induced mice. Same populations were analyzed as shown in Fig. S6a. Only SM14-, SM13-, SM04-, SM03 and SM01-colonized mice were analyzed. All mice remained on a FR diet. Mice were analzyed after 25 days of colonization, representing the timepoint of EAE induction in EAE-induced mice. Colon, ileum, mesenteric lymphnodes and spinal cords were harvested followed by isolation of lymphocytes. Isolated lymphocytes were subjected to FACS-based analysis using the same antibody panels as used for EAE-induced mice.

b): Boxplots of relative abundances of certain T cell populations in various organs. Each dot represents one invidual. Groups are arranged based on their EAE group phenotype classification (**Fig. 5c**): Statistics: only population-organ combinations with statistically significant differences are shown, as calculated by ANOVA. Tukey's honestly significant difference tests (Tukey HSD) were applied to subsequently determine statistical different value distribution between all groups within each population-organ combination. Statistical

differences are indicated by group-assigned letters (a – d). Two groups sharing an assigned letter: $p > 0.05$. Two groups not sharing an assigned letter: $p < 0.05$ (without further distinction).

c): Pearson correlation matrix between group means of certain T cell subsets (vertical) isolated from different organs of non-EAE-induced mice with group means of EAE-associated readouts of EAE-induced mice harboring the same microbiota compositions (SM combinations, irrespective of the diet) as the non-EAE-induced mice. Red squares: significantly different negative correlation, blue squares: significantly different positive correlation. Non-significant correlations not shown. found IL-17$^+$CD4$^+$ and IL-17$^+$IFNγ$^+$CD4$^+$ cell populations in the colonic LP, spinal cords and the ileal LP to correlate significantly. This indicated that the microbiota composition already primed CD4$^+$ T cells into a pro-inflammatory Th17 response before EAE-induction.

d): Hierarchical group clustering of all 5 tested SM combinations based on scaled group means of significantly different T cells subsets, as determined by one-way ANOVA, separated by organ. Color codes indicate corresponding EAE group phenotype in EAE-induced mice, as determined in **Fig. 5c**. Population distribution in the colon aligned best with emerging EAE group phenotypes upon EAE induction, indicating a crucial contribution of T cell priming in the colon by the microbiota to EAE disease course.

EXTENDED FIGURE S6

Microbiota-associated predictors for EAE development

a): Bacterial relative abundances of SM12-, SM13- and SM14-colonized mice, as detected by 16S rRNA gene sequencing, before induction of EAE. No distinction between diets.

b): Linear mixed model regression for predicted maximum score during EAE (MAX) and mean score during relapse phase (Rel Mean) with presence of the strain as an independent variable and colonization as a random intercept effect.

c): Concentrations of secretory IgA, determined from fecal samples and normalized to fecal weights. Fecal samples collected 30 d after EAE induction. Each dot represents one individual mouse. Mice grouped by individual EAE phenotype, as determined in main **Fig. 5e**. Cluster 1: Strong EAE symptoms; Cluster 2: Mild EAE symptoms. Intestinal secretory IgA levels after 30 d of EAE were independent from the respective individual EAE phenotype clusters

d): Concentrations of secretory IgA, determined from fecal samples and normalized to fecal weights. Fecal samples collected 30 d after EAE induction. Each dot represents one individual mouse. Mice grouped by colonization-diet combination and EAE induction status. "- EAE": non-EAE-induced mice. "+ EAE": EAE-induced mice. Intestinal secretory IgA levels after 30 d of EAE were generally higher in mice harboring SM combinations with 12 or more strains.

e): Correlation between susceptibility incidence, as defined in Fig. 1d, in EAE-induced mice harboring a certain SM combination with mean secretory IgA levels in fecal samples obtained from non-EAE-induced mice harboring the same SM combination. Each dot represents one SM combination. Soluble IgA amounts, as detected from fecal samples, were a good predictor for susceptibility to disease upon EAE induction, at least on a group level. However, this finding could not be verified to also apply to individual disease course.

f): IgA-coating index (ICI) of each strain dependent on SM combination. Each dot represents a sample obtained from one individual mouse.

g): Variance in IgA-coating index (ICI) explained by background microbiota compositions in three strains providing highest microbiota-dependencies on ICI.

h): Classification of SM14-constituent strains as IgA high-coated, low-coated or intermediate, dependend on microbiota composition. High coated: ICI > log(2), low coated: ICI < log(0.5), intermediate: log(0.5) < ICI < log(2).

1169 **EXTENDED FIGURE S7**

1170 **EAE scoring scheme**

1171 This scheme shows instructions how daily scoring of mice during EAE disease course was performed. Blue

1172 boxes contain instructions and questions. Arrows show available responses to these questions and orange boxes

1173 show the resulting EAE score.

1174

EXTENDED TABLE 1

Summary and key features of SM14 constituent strains

Abbreviation	Strain	Supplier	Cat#	Phylum
AM	*Akkermansia muciniphila*: DSM 22959, type strain	DSMZ	DSM 22959	*Verrucomicrobia*
BC	*Bacteroides caccae*: DSM 19024, type strain	DSMZ	DSM 19024	*Bacteroidetes*
BO	*Bacteroides ovatus*: DSM 1896, type strain	DSMZ	DSM 1896	*Bacteroidetes*
BT	*Bacteroides thetaiotaomicron*: DSM 2079, type strain	DSMZ	DSM 2079	*Bacteroidetes*
BU	*Bacteroides uniformis*: ATCC 8492, type strain	ATCC	ATCC 8492	*Bacteroidetes*
BI	*Barnesiella intestinihominis*: YIT 11860	DSMZ	DSM 21032	*Bacteroidetes*
CS	*Clostridium symbiosum*: DSM 934, type strain, 2	DSMZ	DSM 934	*Firmicutes*
CA	*Collinsella aerofaciens*: DSM 3979, type strain	DSMZ	DSM 3979	*Actinobacteria*
DP	*Desulfovibrio piger*: ATC 29098, type strain	ATCC	ATC 29098	*Proteobacteria*
EC	*Escherichia coli* HS	ATCC	N/A	*Proteobacteria*
ER	*Eubacterium rectale*: DSM 17629, A1-86	DSMZ	DSM 17629	*Firmicutes*
FP	*Faecalibacterium prausnitzii*: DSM 17677, A2-165	DSMZ	DSM 17677	*Firmicutes*
MF	*Marvinbryantia formatexigens*: DSM 14469, type strain, I-52	DSMZ	DSM 14469	*Firmicutes*
RI	*Roseburia intestinalis*: DSM 14610 type strain, L1-82	DSMZ	DSM 14610	*Firmicutes*

1178 **EXTENDED TABLE 2**

1179 **Summary of primer sequences (5'→3') for strain-specific quantification of bacterial relative**

1180 **abundances**

Strain	Forward primer	Reverse Primer	T_m
AM	GACCGGCATGTTCAAGCAGACT	AAGCCGCATTGGGATTATTTGTT	85.5 °C
BC	GGCGCATGACATTGGAGGTTT	AATACGCCGCATCGCTTTTTC	81.6 °C
BI	ACCGGATTCCTATATTGGGCAGTC	TTCGCTTTTGGCTCTTCCTATTTTC	84.3 °C
BO	GTGAAGGTGCCATCGGAGGAC	GGACGCTTTGGCCACTATTTCA	83.4°C
BT	TACTCGCCTCTTTGCAACCCTACC	GGCCCCAGATCCGAACAACAC	82.8°C
BU	GCTACCGGGAGATACTGGATTGG	TGCGGCGGCCTTTGAAC	84.3°C
CA	GTTCGCGTTCGTTATGGTTGGT	GTTGAGCTGGGCCGATTGTG	89.4°C
CS	CCGCTTGGCATGAAACAGGTATC	TTGGAAGCGGCGAAGAATGG	80.1°C
DP	TGGCTTCAGGCAAATCTCAAAT	TCCGGGGAATCAAAACCATAC	83.1°C
EC	GGTGGCTGGGTGATGTAAAACTGA	ACCGCCGAGCAAAATGAAGC	87.0°C
ER	AGCTTGTGCCGCCCATCTCTAT	TTGCGGTAAAGCTTTGGTGTGG	83.1°C
FP	TGCCCCCGGGTGGTTCT	CGTTATTCAAAGCCCCGTTATCAA	80.1°C
MF	CAGGGATTTTACGTGCTTTATTTTAGTTAT	AGTTCGGATTCGCTCGTATTTTCT	78.6°C
RI	TCGAAATTAAAGAGACGGAAACAGAAG	CCGCTCATATCAATCGAAAACACA	81.9 °C

1181

1182 **EXTENDED TABLE 3:**

1183 **List of metabolites and corresponding KEGG-IDs.**

KEGG	Metabolite	KEGG	Metabolite	KEGG	Metabolite
C00002	ATP	C00140	N-Acetylglucosamine	C00140	N-Acetylglucosamine
C00003	NAD+	C00141	2-Oxoisopentanoate	C00141	2-Oxoisopentanoate
C00004	NADH	C00144	GMP	C00144	GMP
C00006	NADP+	C00147	Adenine	C00147	Adenine
C00008	ADP	C00148	Pro	C00148	Pro
C00015	UDP	C00152	Asn	C00152	Asn
C00016	FAD	C00153	Nicotinamide	C00153	Nicotinamide
C00019	SAM+	C00156	p-Hydroxybenzoate	C00156	p-Hydroxybenzoate
C00020	AMP	C00158	Citrate	C00158	Citrate
C00021	SAH	C00160	Glycolate	C00160	Glycolate
C00024	Acetyl CoA	C00163	Propionate	C00163	Propionate
C00025	Glu	C00167	UDP-glucuronate	C00167	UDP-glucuronate
C00029	UDP-glucose	C00170	5-Methylthioadenosine	C00170	5-Methylthioadenosine
C00037	Gly	C00178	Thymine	C00178	Thymine
C00041	Ala	C00179	Agmatine	C00179	Agmatine
C00042	Succinate	C00183	Val	C00183	Val
C00043	UDP-N-acetylglucosamine	C00186	Lactate	C00186	Lactate
C00047	Lys	C00188	Thr	C00188	Thr
C00049	Asp	C00191	Glucuronate	C00191	Glucuronate
C00055	CMP	C00199	Ru5P	C00199	Ru5P
C00062	Arg	C00206	dADP	C00206	dADP
C00064	Gln	C00212	Adenosine	C00212	Adenosine
C00065	Ser	C00213	Sarcosine	C00213	Sarcosine
C00073	Met	C00214	Thymidine	C00214	Thymidine
C00075	UTP	C00233	4-Methyl-2-oxopentanoate	C00233	4-Methyl-2-oxopentanoate
C00077	Ornithine	C00239	dCMP	C00239	dCMP
C00078	Trp	C00242	Guanine	C00242	Guanine
C00079	Phe	C00245	Taurine	C00245	Taurine
C00082	Tyr	C00246	Butyrate	C00246	Butyrate
C00085	F6P	C00250	Pyridoxal	C00250	Pyridoxal
C00086	Urea	C00253	Nicotinate	C00253	Nicotinate
C00092	G6P	C00257	Gluconate	C00257	Gluconate
C00093	Glycerophosphate	C00258	Glycerate	C00258	Glycerate
C00096	GDP-mannose	C00262	Hypoxanthine	C00262	Hypoxanthine
C00099	beta-Ala	C00263	Homoserine	C00263	Homoserine
C00103	G1P	C00294	Inosine	C00294	Inosine
C00105	UMP	C00299	Uridine	C00299	Uridine
C00106	Uracil	C00300	Creatine	C00300	Creatine
C00112	CDP	C00301	ADP-ribose	C00301	ADP-ribose
C00114	Choline	C00307	CDP-choline	C00307	CDP-choline
C00122	Fumarate	C00311	Isocitrate	C00311	Isocitrate

C00123	Leu	C00314	Pyridoxine	C00314	Pyridoxine
C00127	Glutathione(ox)	C00315	Spermidine	C00315	Spermidine
C00128	CMP-N-acetylneuraminate	C00318	Carnitine	C00318	Carnitine
C00130	IMP	C00327	Citrulline	C00327	Citrulline
C00134	Putrescine(1,4-Butanediamine)	C00329	Glucosamine	C00329	Glucosamine
C00135	His	C00330	2'-Deoxyguanosine	C00330	2'-Deoxyguanosine
C00334	GABA	C00719	Betaine	C02155	Gly-Leu
C00337	Dihydroorotate	C00750	Spermine	C02226	Citraconate
C00346	Ethanolamine phosphate	C00780	Serotonin	C02230	3-Methylguanine
C00355	DOPA	C00785	Urocanate	C02242	7-Methylguanine
C00357	N-Acetylglucosamine 6-phosphate	C00791	Creatinine	C02273	Digalacturonate
C00360	dAMP	C00803	Pentanoate	C02291	Cystathionine
C00363	dTDP	C00818	Saccharate	C02356	2AB
C00364	dTMP	C00842	TDP-glucose	C02378	6-Aminohexanoate
C00366	Urate	C00847	4-Pyridoxate	C02470	Xanthurenate
C00378	Thiamine	C00857	Deamido-NAD+	C02494	1-Methyladenosine
C00380	Cytosine	C00864	Pantothenate	C02504	2-Isopropylmalate
C00383	Malonate	C00879	Mucate	C02567	N1-Acetylspermine
C00385	Xanthine	C00881	2'-Deoxycytidine	C02571	o-Acetylcarnitine
C00387	Guanosine	C00956	alpha-Aminoadipate	C02614	Citramalate
C00388	Histamine	C00979	O-Acetylserine	C02630	2-Hydroxyglutarate
C00407	Ile	C00993	Ala-Ala	C02656	Pimelate
C00408	Pipecolate	C01004	Trigonelline	C02678	Dodecanedioate
C00417	cis-Aconitate	C01005	O-Phosphoserine	C02679	Dodecanoate
C00430	5-Aminolevulinate	C01013	3-Hydroxypropionate	C02693	Indole-3-acetamide
C00431	5-Aminovalerate	C01015	Hydroxyproline	C02704	Methyl sulfate
C00437	N-Acetylornithine	C01026	N,N-Dimethylglycine	C02710	N-Acetylleucine
C00438	Carbamoylaspartate	C01029	N8-Acetylspermidine	C02714	N-Acetylputrescine
C00449	Saccharopine	C01035	gamma-Guanidinobutyrate	C02721	N-Methylalanine
C00455	NMN	C01042	N-Acetylaspartate	C02727	N-epsilon-Acetyllysine
C00475	Cytidine	C01044	N-Formylaspartate	C02835	Imidazole-4-acetate
C00482	Sinapate	C01089	3-Hydroxybutyrate	C02918	1-Methylnicotinamide
C00489	Glutarate	C01104	Trimethylamine N-oxide	C02953	7,8-Dihydrobiopterin
C00491	Cystine	C01118	o-Succinylhomoserine	C02989	Methionine sulfoxide
C00493	Shikimate	C01152	3-Methylhistidine	C02997	N-Acetylhistidine
C00499	Allantoate	C01181	gamma-Butyrobetaine	C03139	Guanidinosuccinate
C00506	Cysteate	C01239	N-Acetylglucosylamine	C03145	N-Formylmethionine
C00519	Hypotaurine	C01262	Anserine	C03264	2-Hydroxy-4-methylpentanoate
C00534	Pyridoxamine	C01494	trans-4-Hydroxy-3-methoxycinnamate	C03283	2,4-Diaminobutyrate
C00581	Guanidinoacetate	C01551	Allantoin	C03406	Argininosuccinate
C00588	Phosphorylcholine	C01571	Decanoate	C03413	N1,N12-Diacetylspermine
C00606	Cysteine sulfinate	C01585	Hexanoate	C03519	N-Acetylphenylalanine
C00612	N1-Acetylspermidine	C01601	Pelargonate	C03626	ADMA
C00624	N-Acetylglutamate	C01606	Phthalate	C03722	2,3-Pyridinedicarboxylate

C00628	2,5-Dihydroxybenzoate	C01620	Threonate	C03752	Glucosaminate
C00630	Isobutyryl CoA	C01672	Cadaverine	C03758	Dopamine
C00631	2PG	C01762	Xanthosine	C03761	3-Hydroxy-3-methylglutarate
C00642	p-Hydroxyphenylacetate	C01879	5-Oxoproline	C03793	N6,N6,N6-Trimethyllysine
C00647	Pyridoxamine 5'-phosphate	C01921	Glycocholate	C04137	Octopine
C00655	XMP	C01987	2-Aminophenol	C04501	N-Acetylglucosamine 1-phosphate
C00669	gamma-Glu-cys	C01996	Acetylcholine	C05122	Taurocholate
C00670	Glycerophosphorylcholine	C02037	Gly-Gly	C05123	Isethionate
C00695	Cholate	C02115	Alpha-Methylserine	C05127	1-Methylhistamine
C00711	Malate	C02129	4-Acetylbutyrate	C02155	Gly-Leu
C05127	1-Methylhistamine	C05824	Cysteine S-sulfate	C08261	Azelate
C05135	4-(beta-Acetylaminoethyl)imidazole	C05984	2-Hydroxybutyrate	C08262	3-Methylbutanoate
C05145	3-Aminoisobutyrate	C06057	3-Aminopropane-1,2-diol	C08277	Sebacate
C05198	5'-Deoxyadenosine	C06337	Terephthalate	C08434	6-Methylaminopurine
C05382	S7P	C06369	2-Deoxyglucose 6-phosphate	C10172	Proline betaine
C05635	5-Hydroxyindoleacetate	C06423	Octanoate	C10833	Syringate
C05771	Isopropanolamine	C06772	Diethanolamine	C16741	5-Hydroxylysine

1184

References:

1. E. Miyauchi, C. Shimokawa, A. Steimle, M. S. Desai, H. Ohno, The impact of the gut microbiome on extra-intestinal autoimmune diseases. *Nat Rev Immunol*, (2022).
2. K. Berer *et al.*, Gut microbiota from multiple sclerosis patients enables spontaneous autoimmune encephalomyelitis in mice. *Proc Natl Acad Sci U S A* **114**, 10719-10724 (2017).
3. S. Miyake *et al.*, Dysbiosis in the Gut Microbiota of Patients with Multiple Sclerosis, with a Striking Depletion of Species Belonging to Clostridia XIVa and IV Clusters. *PLoS One* **10**, e0137429 (2015).
4. A. Duscha *et al.*, Propionic Acid Shapes the Multiple Sclerosis Disease Course by an Immunomodulatory Mechanism. *Cell* **180**, 1067-1080 e1016 (2020).
5. S. Jangi *et al.*, Alterations of the human gut microbiome in multiple sclerosis. *Nat Commun* **7**, 12015 (2016).
6. I. Cosorich *et al.*, High frequency of intestinal TH17 cells correlates with microbiota alterations and disease activity in multiple sclerosis. *Sci Adv* **3**, e1700492 (2017).
7. E. Cekanaviciute *et al.*, Gut bacteria from multiple sclerosis patients modulate human T cells and exacerbate symptoms in mouse models. *Proc Natl Acad Sci U S A* **114**, 10713-10718 (2017).
8. R. E. Ventura *et al.*, Gut microbiome of treatment-naive MS patients of different ethnicities early in disease course. *Sci Rep* **9**, 16396 (2019).
9. D. Takewaki *et al.*, Alterations of the gut ecological and functional microenvironment in different stages of multiple sclerosis. *Proc Natl Acad Sci U S A* **117**, 22402-22412 (2020).
10. C. Ballerini, Experimental Autoimmune Encephalomyelitis. *Methods Mol Biol* **2285**, 375-384 (2021).
11. E. Miyauchi *et al.*, Gut microorganisms act together to exacerbate inflammation in spinal cords. *Nature* **585**, 102-106 (2020).
12. J. Ochoa-Reparaz *et al.*, A polysaccharide from the human commensal Bacteroides fragilis protects against CNS demyelinating disease. *Mucosal Immunol* **3**, 487-495 (2010).
13. A. Mangalam *et al.*, Human Gut-Derived Commensal Bacteria Suppress CNS Inflammatory and Demyelinating Disease. *Cell Rep* **20**, 1269-1277 (2017).
14. E. Cekanaviciute *et al.*, Multiple Sclerosis-Associated Changes in the Composition and Immune Functions of Spore-Forming Bacteria. *mSystems* **3**, (2018).
15. M. S. Desai *et al.*, A Dietary Fiber-Deprived Gut Microbiota Degrades the Colonic Mucus Barrier and Enhances Pathogen Susceptibility. *Cell* **167**, 1339-1353 e1321 (2016).
16. M. Neumann *et al.*, Deprivation of dietary fiber in specific-pathogen-free mice promotes susceptibility to the intestinal mucosal pathogen Citrobacter rodentium. *Gut Microbes* **13**, 1966263 (2021).
17. M. Van der Sluis *et al.*, Muc2-deficient mice spontaneously develop colitis, indicating that MUC2 is critical for colonic protection. *Gastroenterology* **131**, 117-129 (2006).
18. E. C. Martens, M. Neumann, M. S. Desai, Interactions of commensal and pathogenic microorganisms with the intestinal mucosal barrier. *Nat Rev Microbiol* **16**, 457-470 (2018).
19. S. Liu *et al.*, Oral Administration of miR-30d from Feces of MS Patients Suppresses MS-like Symptoms in Mice by Expanding Akkermansia muciniphila. *Cell Host Microbe* **26**, 779-794 e778 (2019).
20. A. Steimle *et al.*, Constructing a gnotobiotic mouse model with a synthetic human gut microbiome to study host–microbe cross talk. *STAR Protocols* **2**, (2021).
21. J. Singh *et al.*, Urinary and Plasma Metabolomics Identify the Distinct Metabolic Profile of Disease State in Chronic Mouse Model of Multiple Sclerosis. *J Neuroimmune Pharmacol* **14**, 241-250 (2019).
22. L. M. Poisson *et al.*, Untargeted Plasma Metabolomics Identifies Endogenous Metabolite with Drug-like Properties in Chronic Animal Model of Multiple Sclerosis. *J Biol Chem* **290**, 30697-30712 (2015).
23. D. M. Johanson, 2nd *et al.*, Experimental autoimmune encephalomyelitis is associated with changes of the microbiota composition in the gastrointestinal tract. *Sci Rep* **10**, 15183 (2020).
24. Y. Rao *et al.*, Gut Akkermansia muciniphila ameliorates metabolic dysfunction-associated fatty liver disease by regulating the metabolism of L-aspartate via gut-liver axis. *Gut Microbes* **13**, 1-19 (2021).
25. M. Lopez-Siles, S. H. Duncan, L. J. Garcia-Gil, M. Martinez-Medina, Faecalibacterium prausnitzii: from microbiology to diagnostics and prognostics. *ISME J* **11**, 841-852 (2017).
26. M. C. E. a. s. b. u. e. i, M. C. i, Gut microbiome of multiple sclerosis patients and paired household healthy controls reveal associations with disease risk and course. *Cell* **185**, 3467-3486 e3416 (2022).

27. N. Feizi *et al.*, CD8(+) T cells specific for cryptic apoptosis-associated epitopes exacerbate experimental autoimmune encephalomyelitis. *Cell Death Dis* **12**, 1026 (2021).
28. O. L. Rojas *et al.*, Recirculating Intestinal IgA-Producing Cells Regulate Neuroinflammation via IL-10. *Cell* **176**, 610-624 e618 (2019).
29. A. Mathias, B. Pais, L. Favre, J. Benyacoub, B. Corthesy, Role of secretory IgA in the mucosal sensing of commensal bacteria. *Gut Microbes* **5**, 688-695 (2014).
30. A. Pu, D. S. W. Lee, B. Isho, I. Naouar, J. L. Gommerman, The Impact of IgA and the Microbiota on CNS Disease. *Front Immunol* **12**, 742173 (2021).
31. A. K. Probstel *et al.*, Gut microbiota-specific IgA(+) B cells traffic to the CNS in active multiple sclerosis. *Sci Immunol* **5**, (2020).
32. N. W. Palm *et al.*, Immunoglobulin A coating identifies colitogenic bacteria in inflammatory bowel disease. *Cell* **158**, 1000-1010 (2014).
33. S. K. Tankou *et al.*, Investigation of probiotics in multiple sclerosis. *Mult Scler* **24**, 58-63 (2018).
34. M. Wolter *et al.*, Leveraging diet to engineer the gut microbiome. *Nat Rev Gastroenterol Hepatol* **18**, 885-902 (2021).
35. K. Rawat, N. Singh, P. Kumari, L. Saha, A review on preventive role of ketogenic diet (KD) in CNS disorders from the gut microbiota perspective. *Rev Neurosci* **32**, 143-157 (2021).
36. K. F. Al *et al.*, Fecal microbiota transplantation is safe and tolerable in patients with multiple sclerosis: A pilot randomized controlled trial. *Mult Scler J Exp Transl Clin* **8**, 20552173221086662 (2022).
37. S. N. Choileain *et al.*, CXCR3+ T cells in multiple sclerosis correlate with reduced diversity of the gut microbiome. *J Transl Autoimmun* **3**, 100032 (2020).
38. T. M. Greiling *et al.*, Commensal orthologs of the human autoantigen Ro60 as triggers of autoimmunity in lupus. *Sci Transl Med* **10**, (2018).
39. J. Wang *et al.*, HLA-DR15 Molecules Jointly Shape an Autoreactive T Cell Repertoire in Multiple Sclerosis. *Cell* **183**, 1264-1281 e1220 (2020).
40. P. D. Cani, W. M. de Vos, Next-Generation Beneficial Microbes: The Case of Akkermansia muciniphila. *Front Microbiol* **8**, 1765 (2017).
41. B. Routy *et al.*, Gut microbiome influences efficacy of PD-1-based immunotherapy against epithelial tumors. *Science* **359**, 91-97 (2018).
42. R. Bhat *et al.*, Inhibitory role for GABA in autoimmune inflammation. *Proc Natl Acad Sci U S A* **107**, 2580-2585 (2010).
43. N. Yalcinkaya *et al.*, Reduced fecal GABA levels in multiple sclerosis patients. *Mult Scler Relat Disord* **9**, 60-61 (2016).
44. N. P. Hyland, J. F. Cryan, A Gut Feeling about GABA: Focus on GABA(B) Receptors. *Front Pharmacol* **1**, 124 (2010).
45. P. Strandwitz *et al.*, GABA-modulating bacteria of the human gut microbiota. *Nat Microbiol* **4**, 396-403 (2019).
46. K. Z. Coyte, S. Rakoff-Nahoum, Understanding Competition and Cooperation within the Mammalian Gut Microbiome. *Curr Biol* **29**, R538-R544 (2019).
47. K. Faust *et al.*, Signatures of ecological processes in microbial community time series. *Microbiome* **6**, 120 (2018).
48. A. L. Gould *et al.*, Microbiome interactions shape host fitness. *Proc Natl Acad Sci U S A* **115**, E11951-E11960 (2018).
49. S. Rakoff-Nahoum, K. R. Foster, L. E. Comstock, The evolution of cooperation within the gut microbiota. *Nature* **533**, 255-259 (2016).
50. S. F. Henriques *et al.*, Metabolic cross-feeding in imbalanced diets allows gut microbes to improve reproduction and alter host behaviour. *Nat Commun* **11**, 4236 (2020).
51. A. Steimle, M. Neumann, E. T. Grant, J. D. Turner, M. S. Desai, Concentrated Raw Fibers Enhance the Fiber-Degrading Capacity of a Synthetic Human Gut Microbiome. *Int J Mol Sci* **22**, (2021).
52. J. J. Kozich, S. L. Westcott, N. T. Baxter, S. K. Highlander, P. D. Schloss, Development of a dual-index sequencing strategy and curation pipeline for analyzing amplicon sequence data on the MiSeq Illumina sequencing platform. *Appl Environ Microbiol* **79**, 5112-5120 (2013).

53. P. D. Schloss *et al.*, Introducing mothur: open-source, platform-independent, community-supported software for describing and comparing microbial communities. *Appl Environ Microbiol* **75**, 7537-7541 (2009).
54. A. Steimle, E. T. Grant, M. S. Desai, Quantitative assay to detect bacterial glycan-degrading enzyme activities in mouse and human fecal samples. *STAR Protoc* **2**, 100326 (2021).
55. M. C. Buscarinu *et al.*, Altered intestinal permeability in patients with relapsing-remitting multiple sclerosis: A pilot study. *Mult Scler* **23**, 442-446 (2017).
56. J. D. Glenn, E. M. Mowry, Emerging Concepts on the Gut Microbiome and Multiple Sclerosis. *J Interferon Cytokine Res* **36**, 347-357 (2016).
57. K. Kasahara *et al.*, Interactions between Roseburia intestinalis and diet modulate atherogenesis in a murine model. *Nat Microbiol* **3**, 1461-1471 (2018).
58. G. P. Rodriguez-Castano *et al.*, Bacteroides thetaiotaomicron Starch Utilization Promotes Quercetin Degradation and Butyrate Production by Eubacterium ramulus. *Front Microbiol* **10**, 1145 (2019).
59. A. Haghikia *et al.*, Dietary Fatty Acids Directly Impact Central Nervous System Autoimmunity via the Small Intestine. *Immunity* **43**, 817-829 (2015).

Figure 1

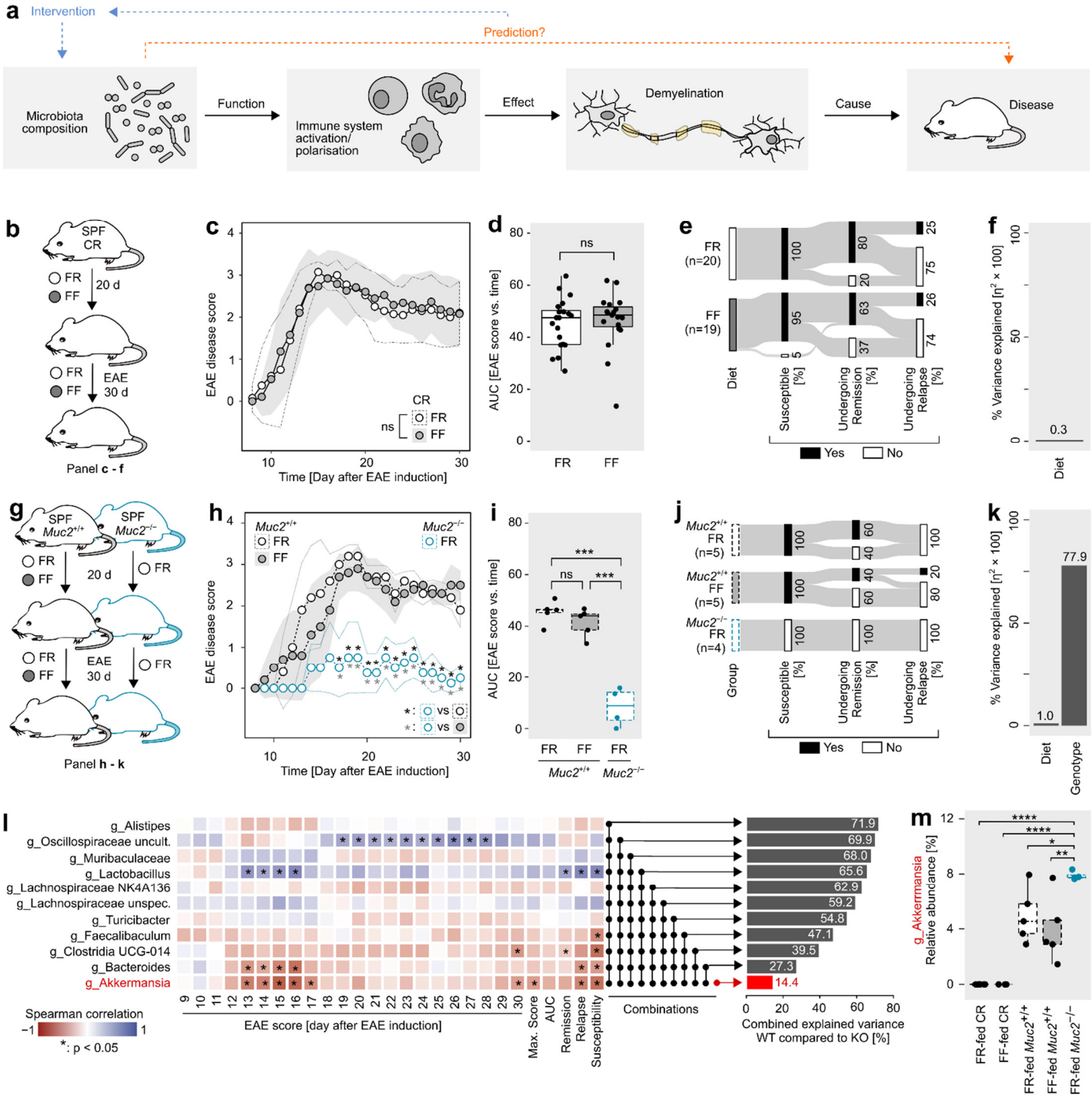

Figure 2

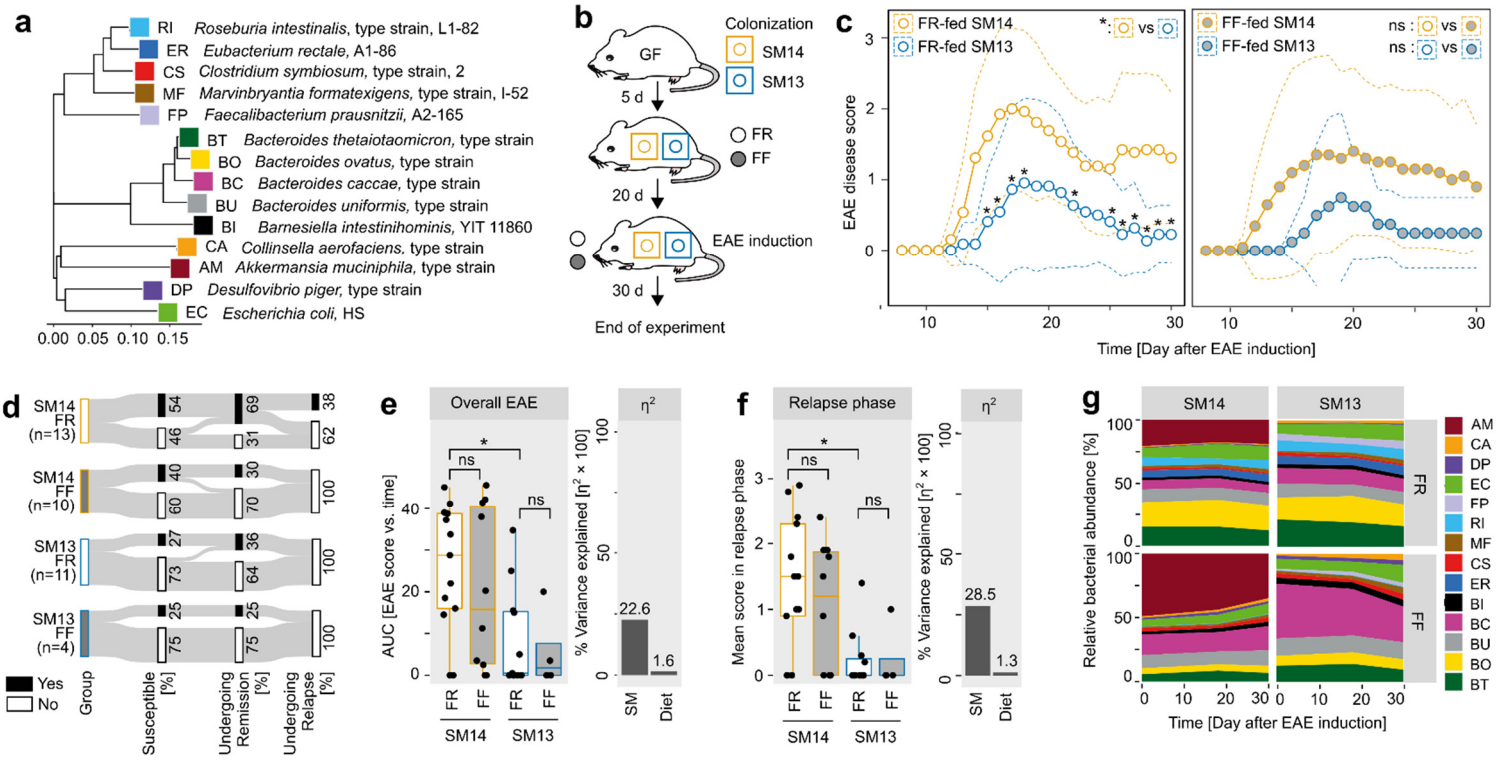

Figure 3

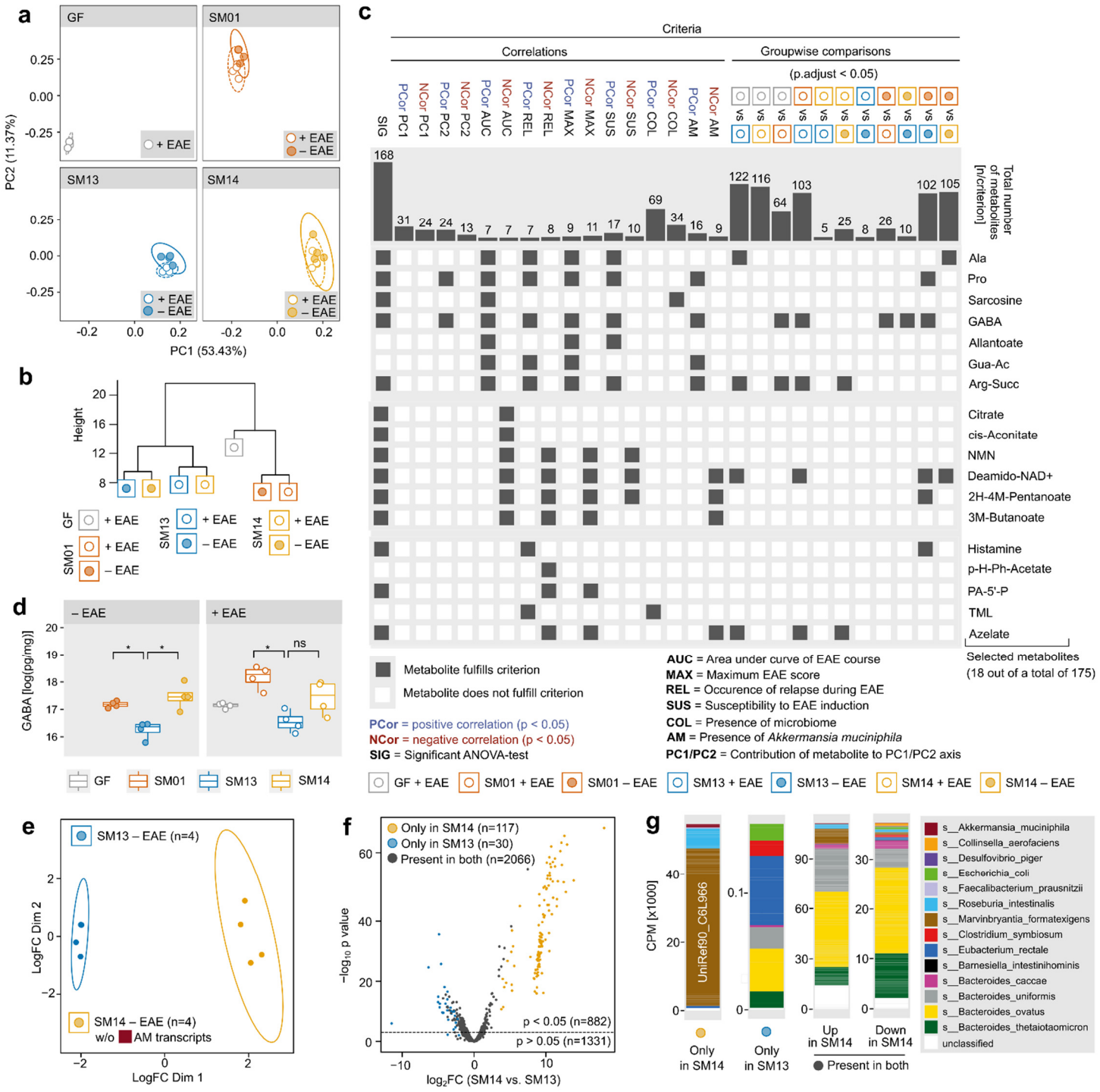

Figure 4

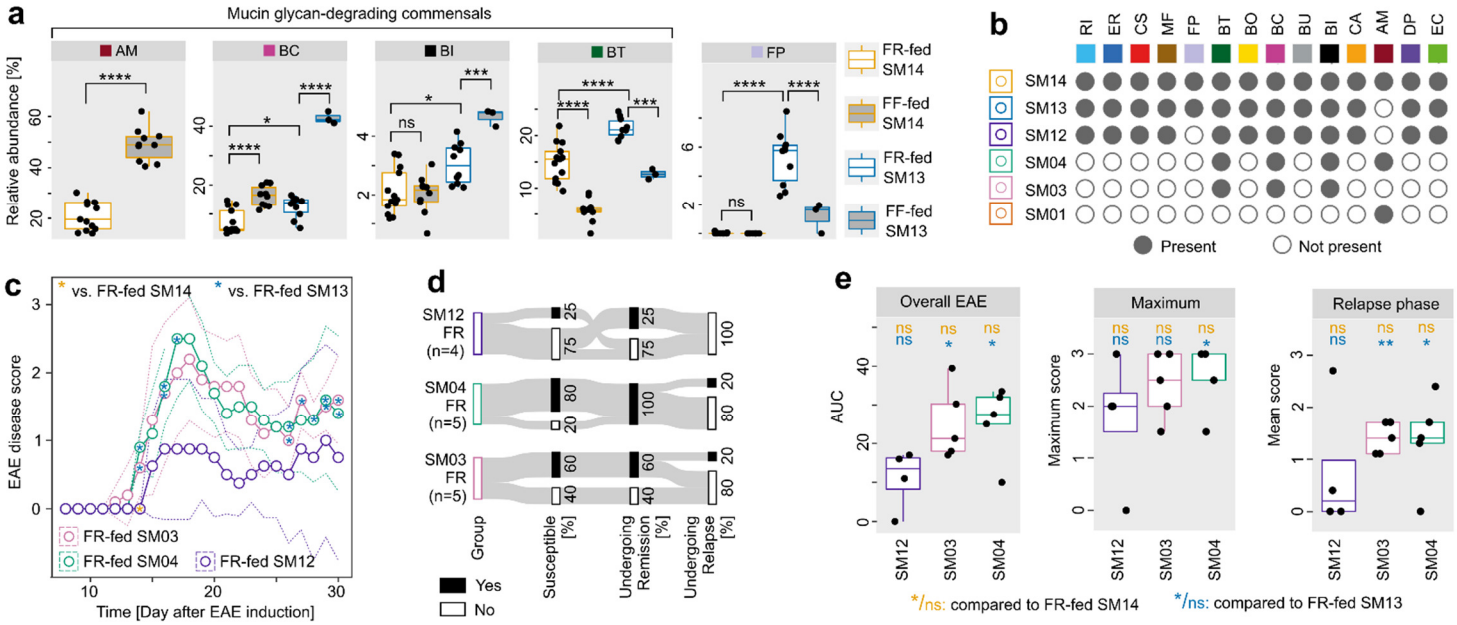

Figure 5

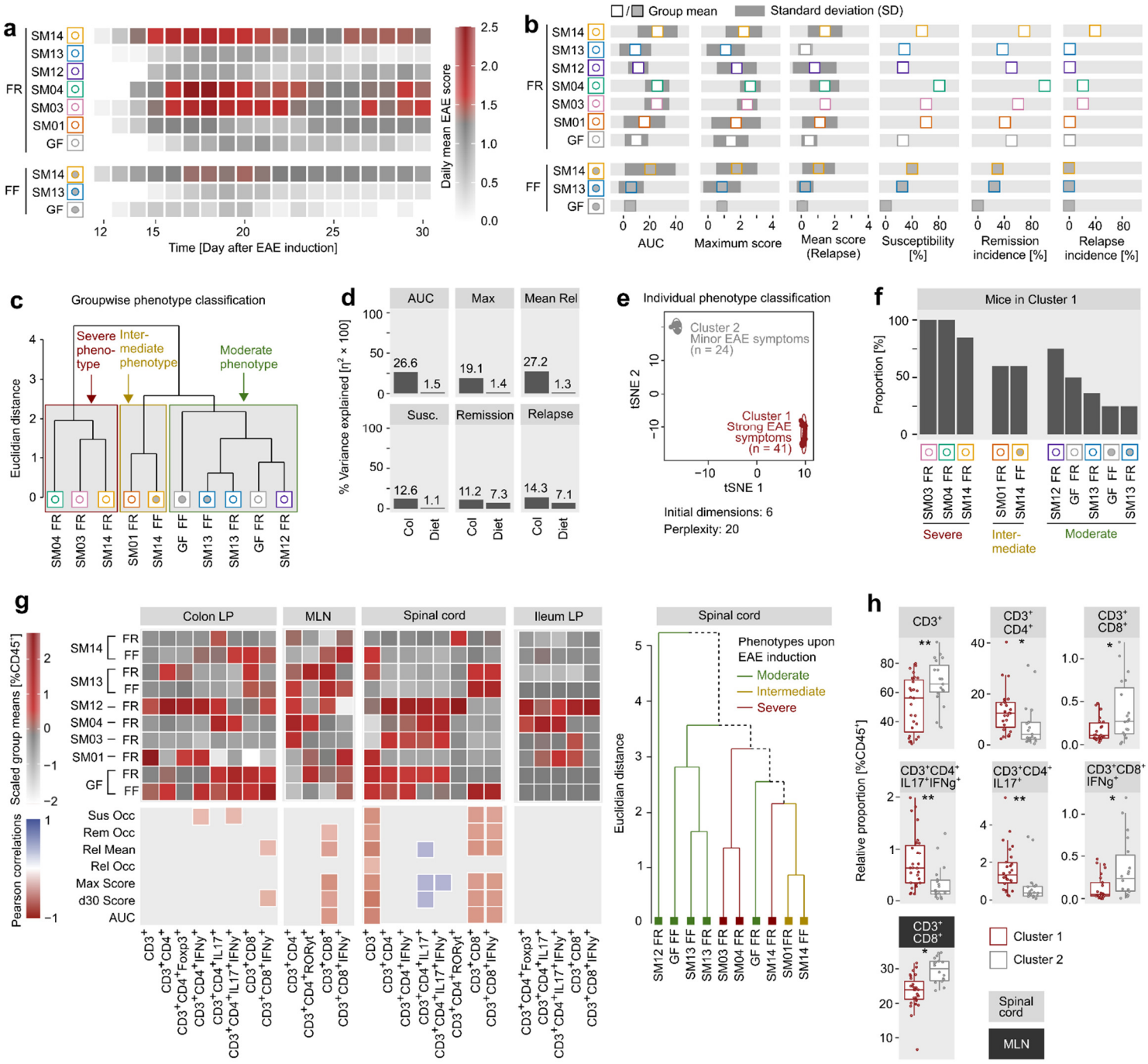

Figure 6

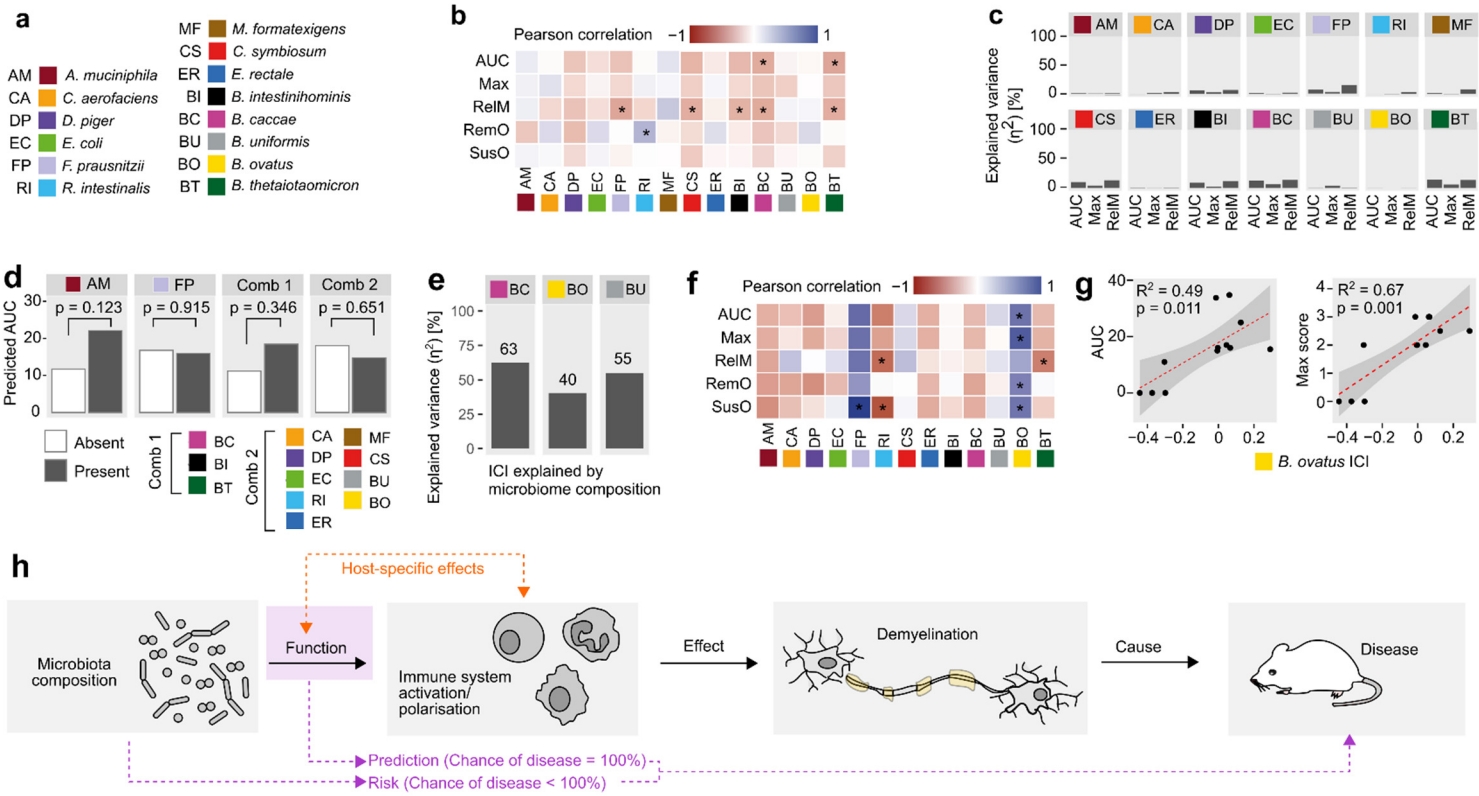

Extended Figure S1

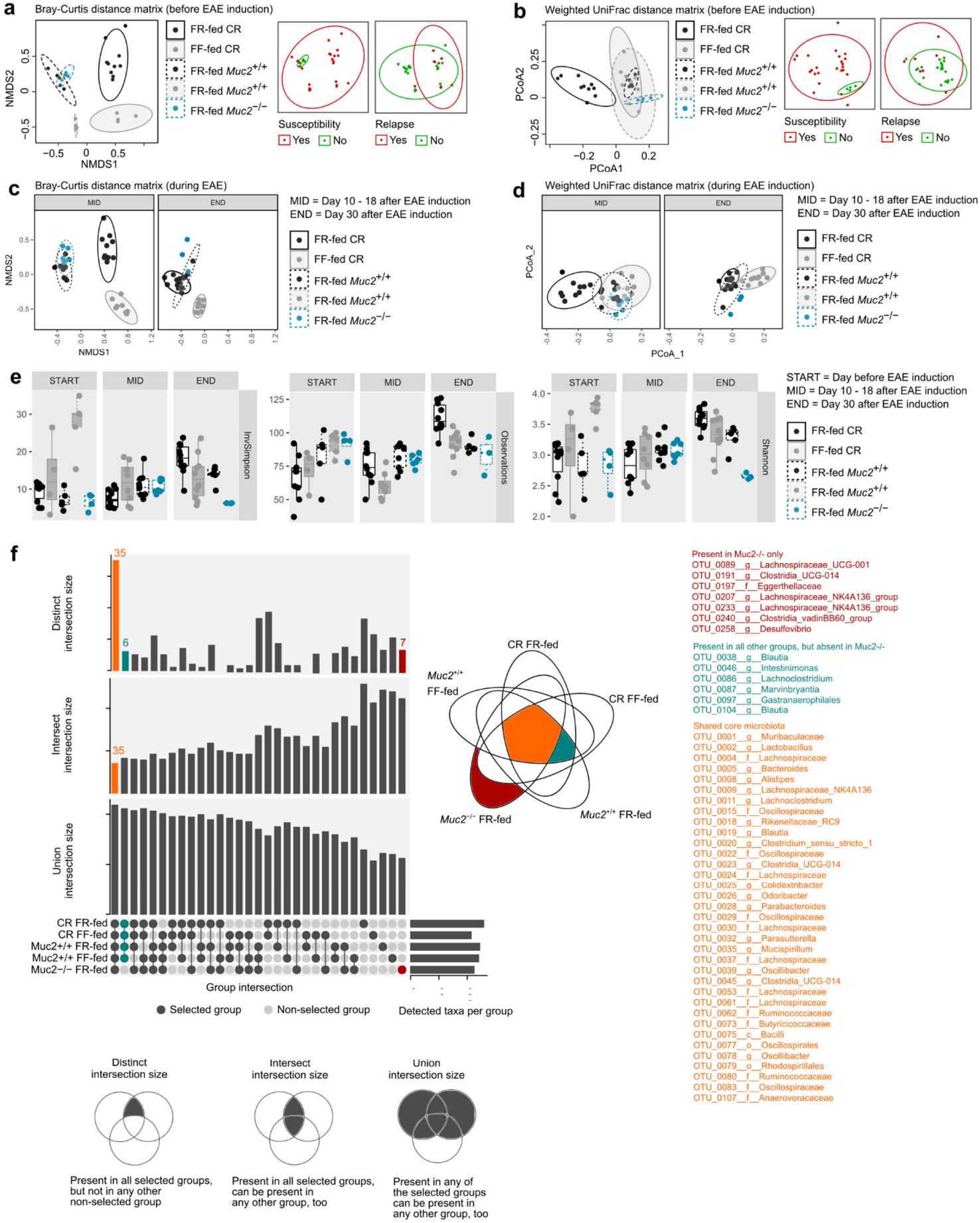

Extended figure S2

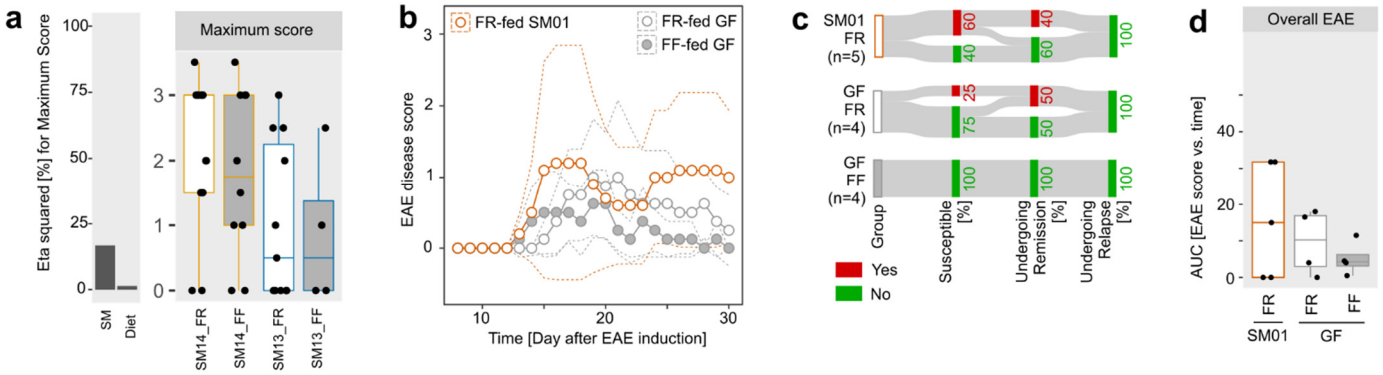

Extended figure S3

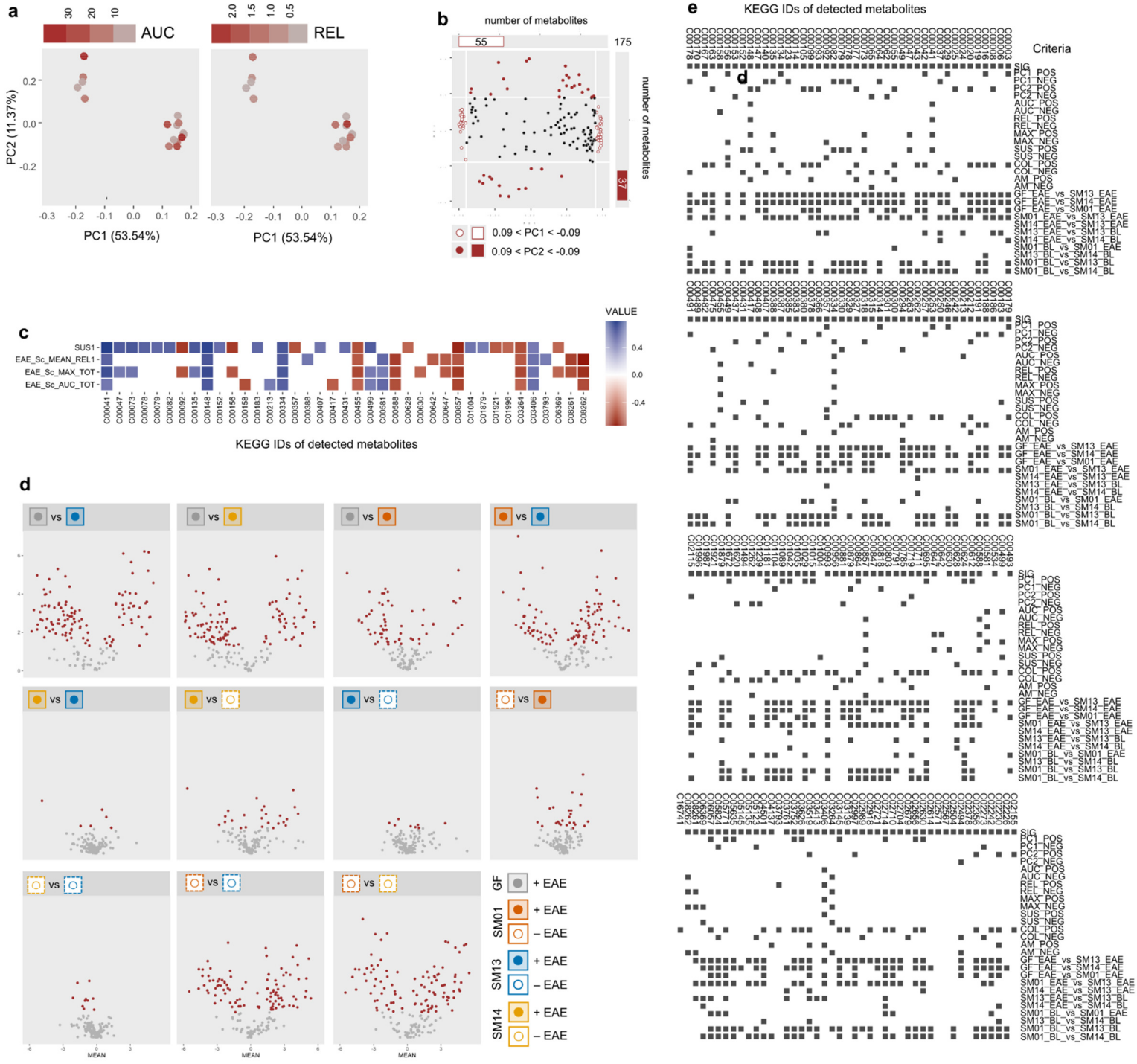

Extended Figure S4

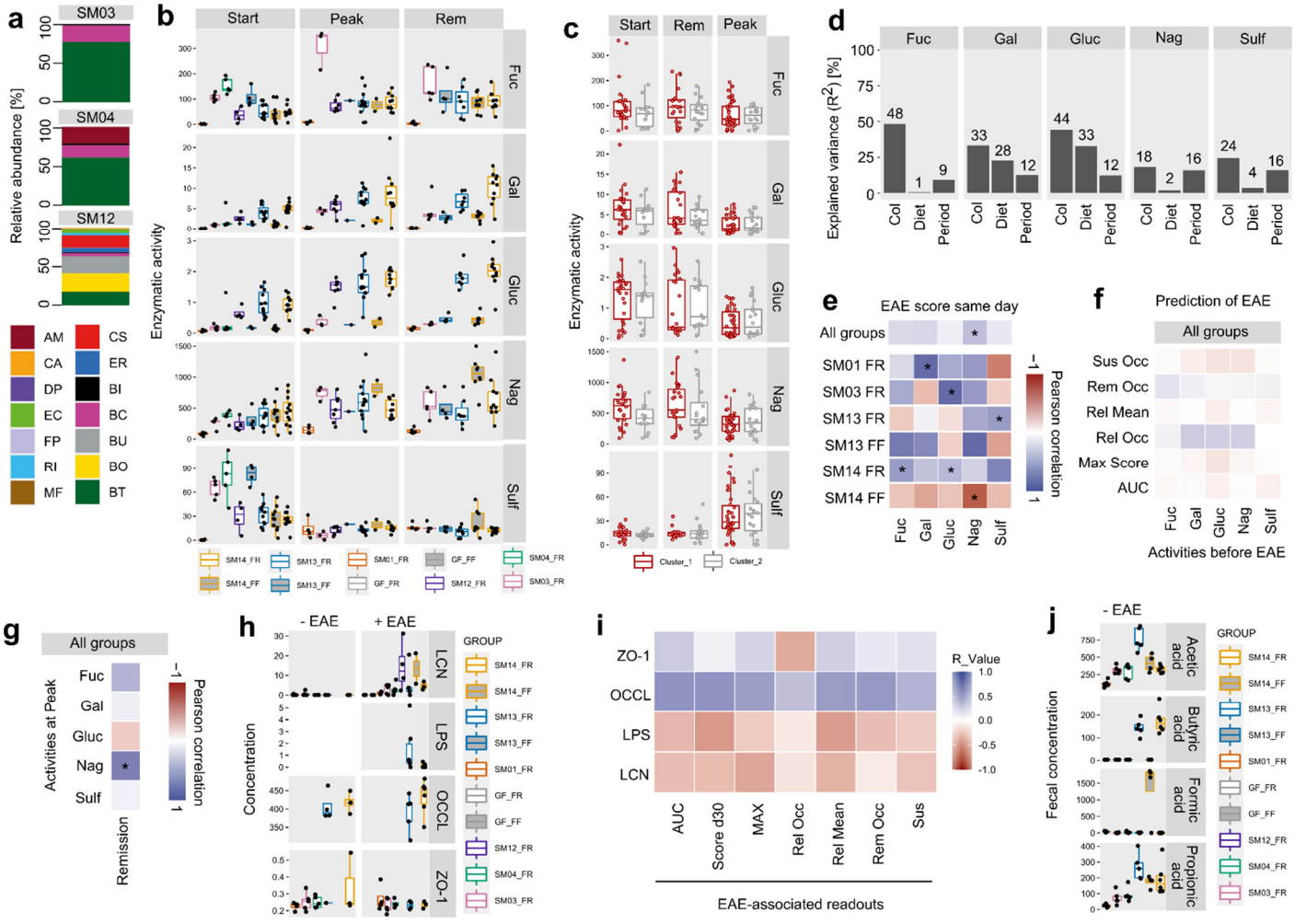

Extended figure S5

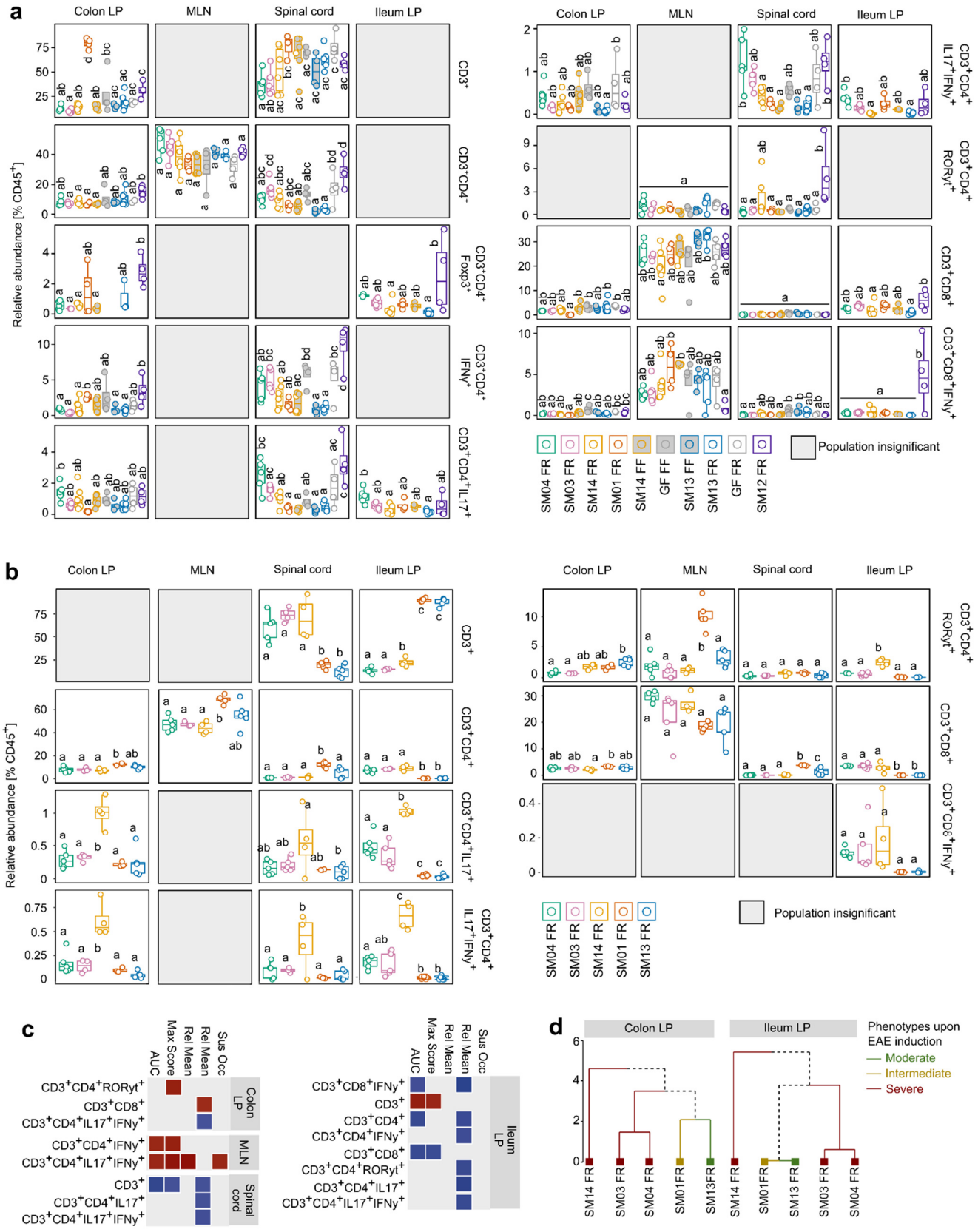

Extended figure S6

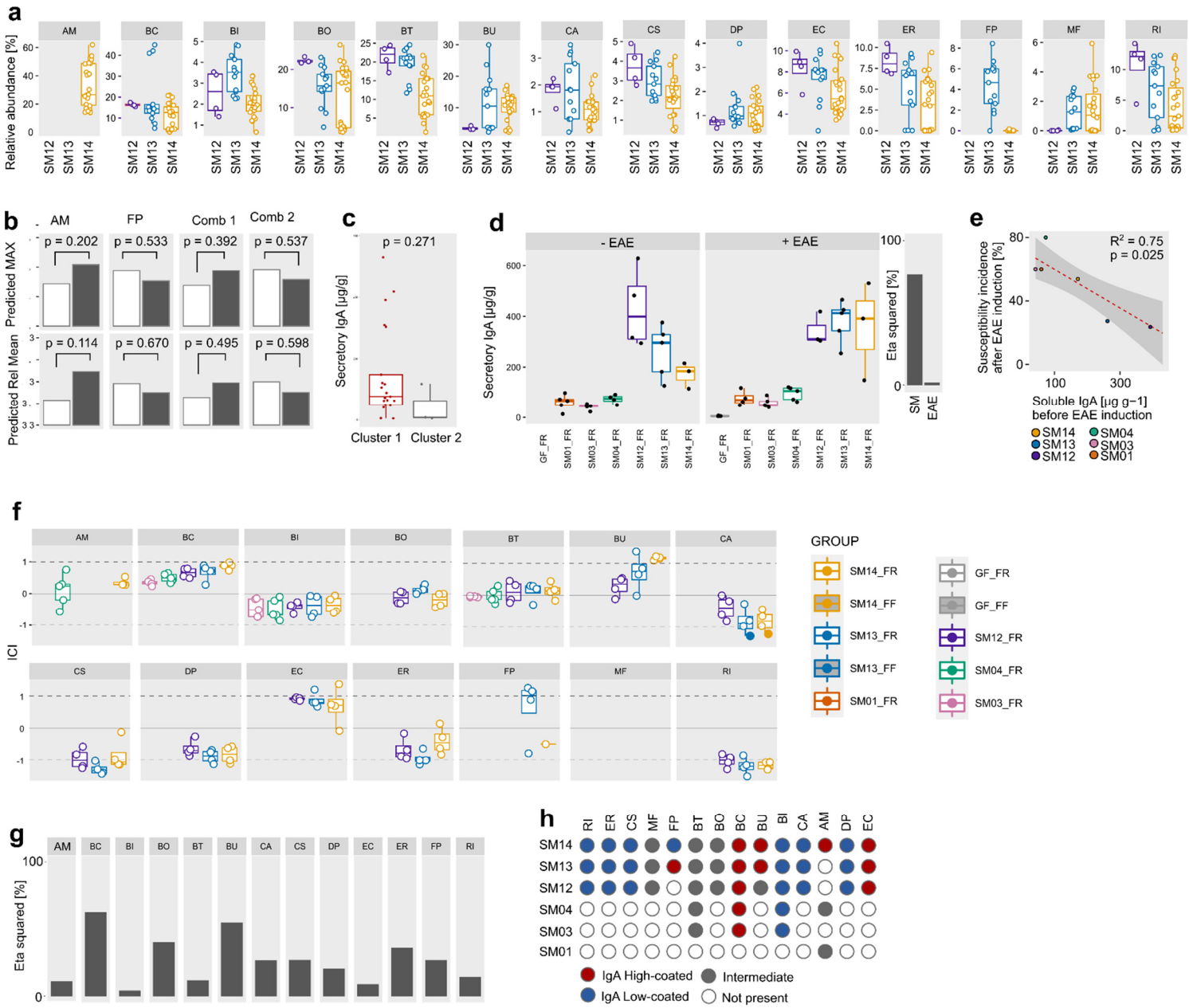

Extended figure S7